Geophysical Journal International

Geophys. J. Int. (2011) **187,** 178–198 doi: 10.1111/j.1365-246X.2011.05123.x

Periodicity, chaos and localization in a Burridge–Knopoff model of an earthquake with rate-and-state friction

Brittany A. Erickson,[1] Björn Birnir[2] and Daniel Lavallée[3]

[1]*Department of Geophysics, Stanford University, Stanford, CA, USA. E-mail: baericks@stanford.edu*
[2]*Department of Mathematics, University of California, Santa Barbara, CA, USA.*
[3]*Earth Research Institute, University of California, Santa Barbara, CA, USA.*

Accepted 2011 June 23. Received 2011 June 13; in original form 2010 August 31

GJI Marine geosciences and applied geophysics

SUMMARY

We investigate the emergent dynamics when the slip law formulation of the non-linear rate-and-state friction law is attached to a Burridge–Knopoff spring-block model. We derive both the discrete equations and the continuum formulation governing the system in this framework. The discrete system (ODEs) exhibits both periodic and chaotic motion, where the system's transition to chaos is size-dependent, that is, how many blocks are considered. From the discrete model we derive the non-linear elastic wave equation by taking the continuum limit. This results in a non-linear partial differential equation (PDE) and we find that chaos ensues when the same parameter is increased. This critical parameter value needed for the onset of chaos in the continuous model is much smaller than the value needed in the case of a single block and we discuss the implications this has on dynamic modelling of earthquake rupture with this specific friction law. Most importantly, these results suggest that the friction law is scale-dependent, thus caution should be taken when attaching a friction law derived at laboratory scales to full-scale earthquake rupture models. Furthermore, we find solutions where the initial slip pulse propagates like a travelling wave, or remains localized in space, suggesting the presence of soliton and breather solutions. We discuss the significance of these pulse-like solutions and how they can be understood as a proxy for the propagation of the rupture front across the fault surface during an earthquake. We compute analytically the conditions for soliton solutions and by exploring the resulting parameter space, we introduce a possible method for determining a range of suitable parameter values to be used in future dynamic earthquake modelling.

Key words: Numerical solutions; Non-linear differential equations; Friction; Earthquake dynamics.

1 INTRODUCTION

1.1 Background

Although significant advances have been made in our knowledge of fault structure and plate tectonics, our understanding of the the physical mechanisms responsible for the initiation, propagation and termination of earthquake rupture remains unclear. It is believed that there exist complex physical properties and behaviours in the earth's crust and along fault surfaces that prevent our ability to make accurate predictions. Two avenues by which we try to understand the physics and complexity of earthquakes are in laboratory studies of rock friction and mathematical dynamic rupture modelling. So far these two fields remain relatively disconnected and it is still unclear how laboratory discoveries can best be applied in dynamic models of earthquake faults (Scholz 1998; Marone 1998).

The late 1970s saw an increased interest in stick-slip instabilities present in laboratory rock experiments as a means of understanding earthquake ruptures. Dieterich, Ruina, Rice and others used these experiments as a means to formulate constitutive laws capable of describing the frictional stress when rocks were sheared against each other or over a surface (Dieterich 1978; Rice 1983; Ruina 1983). The mechanisms of slip instabilities in laboratory experiments have been proposed to be dependent on several factors including reduced frictional force during sliding (slip weakening) or accompanying an increase in slip velocity (rate weakening) (Ruina 1983). Improvements to these constitutive laws were made when data analysis suggested that friction could not be a function solely dependent on velocity, nor could slip-weakening friction completely describe the relationship between static and dynamic friction (Marone 1998).

Resolution to these setbacks were made when they found that with the incorporation of a state variable there emerged a robust friction law capable of reproducing a wide range of dynamics similar to the behaviour of a fault during an earthquake rupture. These emergent dynamics include a Gutenberg–Richter distribution of event sizes, stick-slip phenomena and fault healing (Marone 1998). The state variable is an empirical quantity usually interpreted as a measure of asperity contact between two sheared surfaces, or the amount of time required for the renewal of these asperities (characteristic contact lifetime) (Marone 1998).

1.2 The 'slip law' formulation

In the literature this constitutive law is currently referred to as 'rate-and-state' friction with the specific state evolution law often referred to by author name. One formulation of such a friction law was proposed by Ruina (1983) and is known as the 'Ruina law' or 'slip law' (Dieterich 1979; Ruina 1983; Marone 1998)

$$\left.\begin{aligned} \tau &= \sigma_n\left[f^* + b\ln\left(\tfrac{v_o\theta}{D_c}\right) + a\ln\left(\tfrac{v}{v_o}\right)\right] \\ \tfrac{d\theta}{dt} &= -\tfrac{v\theta}{D_c}\ln\left(\tfrac{v\theta}{D_c}\right) \end{aligned}\right\}, \quad (1)$$

where the friction stress τ is a function of the normal stress σ_n, f^* is the steady-state coefficient of friction when sliding at velocity v_o (Marone 1998) and introduced for dimensional consistency (Ruina 1983), D_c is the critical slip distance in order for friction to change from static to dynamic values (Rabinowicz 1951), v is the slip rate, a and b are positive frictional parameters that scale the response to a step change in the imposed velocity of a single spring-block configuration (Scholz 2002) (see Fig. 1 where $A = \sigma_n a$ and $B = \sigma_n b$) and θ is the state variable. And while there are other formulations of the state evolution law for rate-and-state friction and none can completely simulate all the laboratory data of friction, the studies conducted by Ampuero & Rubin (2007) (and references therein) suggest that the slip law is far more consistent with laboratory experiments of velocity stepping as described in Fig. 1.

According to Dieterich & Kilgore (1994), the parameter D_c corresponds to the critical sliding distance necessary to replace the population of asperity contacts. Setting $A = \sigma_n a$ and $B = \sigma_n b$, the meaning of these two parameters is best understood by writing the expression for the friction stress

$$\tau = \tau_0 + B\ln\left(\frac{v_0\theta}{D_c}\right) + A\ln\left(\frac{v}{v_0}\right),$$

where τ_0 is the traction when the slider is moving at constant velocity v_o. When the slider moves at constant velocity v_{ss} (steady state), the expression for the stress becomes

$$\tau_{ss} = \tau_0 - (B - A)\ln(v_{ss}/v_0).$$

According to Rice (1983) and Rice *et al.* (2001), the parameter $A = \partial\tau/\partial\ln(v)$ is a measure of the direct velocity dependence (sometimes called the 'direct effect') while $(A - B) = \partial\tau_{ss}/\partial\ln(v_{ss})$ is a measure of the steady-state velocity dependence (see Fig. 1). Furthermore, if the slip velocity v can be approximated by a step function then the parameter $(B - A)$ plays a role of a stress drop while A corresponds to the strength excess (Ohnaka & Shen 1999) and are related to the non-dimensional seismic ratio S that affects supershear rupture (Andrews 1976; Dunham 2007; Schmedes *et al.* 2010b) by the following relation $S = \frac{A}{B-A}$.

1.3 The Burridge–Knopoff model

The ability of rate-and-state friction to properly reproduce earthquake dynamics is studied by the formulation of a dynamic rupture model subject to a friction law, an initial spatial distribution of the stress and strength of the material over the fault surfaces, as well as a mathematical description of how these properties evolve during the rupture process. One type of dynamic model, studied extensively since its introduction in the 1960s, is the Burridge & Knopoff (1967) (BK) model of many blocks interconnected by elastic springs (see Fig. 2) with spring stiffness coefficient μ. The blocks are also elastically coupled (with spring stiffness coefficient λ) to a rigid plate moving at a constant velocity v_p and pulled over a rough surface described by some friction law. The interface between the blocks and the rough surface can be considered an analogue for a 1-D earthquake fault (Carlson *et al.* 1991).

Although there are more physical rupture models available [for a comprehensive review of numerical implementations of dynamic modelling of earthquake rupture see Section 2 of Madariaga & Olsen (2002) and references therein], the simplicity of the BK model allows for the numerical simulation of a large number of scenarios

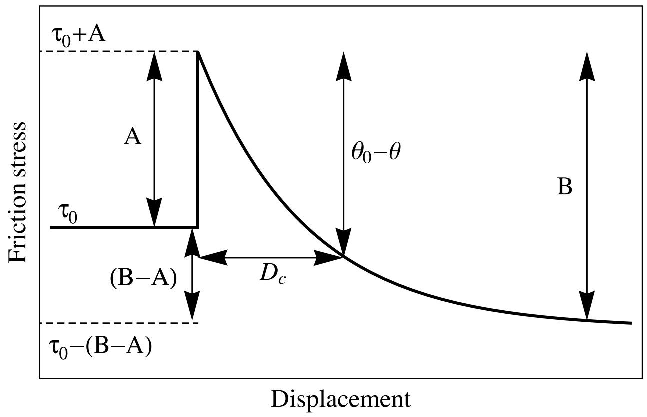

Figure 1. Schematic diagram taken from Erickson *et al.* (2008) [originally from Scholz (2002)], illustrating the response to a step change in the imposed velocity, v of a single spring-block slider model. The imposed velocity, initially maintained constant at v_0, is suddenly incremented by a factor of v_0 (denoted by Δv) and subsequently held constant at $v_0 + \Delta v$. The friction stress τ, initially constant at τ_0, suddenly increases by A when the velocity is incremented by Δv and then decreases exponentially to B. The length scale D_c, characterizes the distance taken by the state variable θ to reach a new steady state θ_0.

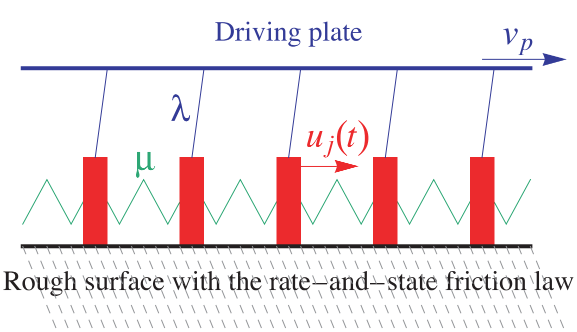

Figure 2. The equations of motion are derived from the dynamics of a spring connected chain of blocks, elastically coupled to a driver plate moving at a constant velocity v_p. $u_j(t)$ is the slip value of the jth block, μ is the spring coefficient between blocks and λ corresponds to the elastic coupling with the driver plate. The blocks slide along the rough surface according to a particular friction law (rate-and-state friction for this study). Depending on the values of the internal parameters, the chain will move in a variety of ways.

and thus a larger exploration of the parameter space characterizing the rate-and-state friction law.

Burridge & Knopoff (1967) conducted several laboratory experiments of this system—the first case considered equal spring constants between blocks, and the second with graduated values for the spring constants. They observed several types of behaviour in this configuration including the presence of large shocks in the system when the spring constants were stretched far enough to set the blocks on the verge of instability. And while they found a Gutenberg–Richter distribution of event sizes present in their model, they note that statistical properties along the fault surface are determined by the nature of the friction law describing the interface (a property confirmed, at least partially, by Elbanna & Heaton 2009). At this time rate-and-state friction laws had not yet emerged as powerful tools in dynamic simulations however. Burridge and Knopoff formulated the equations of motion for this system incorporating a friction law that was dependent only on the block's velocity.

These equations and similar formulations of them have been studied in detail since this time. In studies involving a velocity weakening friction law attached to a BK model, the internal parameter space has been explored and a rich variety of dynamics have been observed including chaotic regimes as well as localized solutions, see (Carlson *et al.* 1991; Schmittbuhl *et al.* 1993, 1996; Español 1994; Elbanna & Heaton 2009). Carlson & Langer (1989) considered a spring-block model under a velocity weakening friction law: if X_j is the position of the jth block and the slip rate v is denoted by $\dot{X}_j$, then the friction acting on this particle is given by

$$F(\dot{X}_j) = F_o \phi(\dot{X}_j / v_1), \tag{2}$$

where v_1 is a characteristic speed and ϕ vanishes for large values of $\dot{X}_j$ and is normalized so that $\phi(0) = -\phi'(0) = 1$. They found that this friction law exhibits periodic as well as stick-slip motion in the spring-block system. Furthermore, Carlson *et al.* (1991) found a transition from localized to delocalized events and derived a parameter condition for the BK model under velocity-weakening friction that guarantees that pulses remained sufficiently small so as not to propagate into the outer, firmly stuck regions in the model. In Schmittbuhl *et al.* (1993), the authors found a wide range of event types by varying a control parameter proportional to the product of the driving rate and the size of the system. The authors found that by increasing the parameter $N \times v_p$, (the product of the size of the system or number of blocks, N and v_p, the driving displacement rate), a transition from chaotic to localized (solitary wave type) solutions occurred (referred to as a 'finite-size effect'). When $N \times v_p = 8$, for example, a solitary wave emerged with constant speed (10 blocks per time unit) and a wavelength of eight blocks. Furthermore, the work of Español (1994) studied a BK model of a spring-block system subject to velocity weakening friction. For slip rate v,

$$F(v) = \frac{F_o}{1 + \frac{v}{v_f}}, \tag{3}$$

where v_f is a characteristic velocity for friction and F_o is the threshold friction. In their model, the speed of sound, l is defined by the ratio of the spring constant between the blocks and the spring constant connecting the block to the driver plate ($l^2 = \frac{\mu}{\lambda}$ for the parameters described in Fig. 2). By varying the speed of sound, they observed intervals in which periodic, complex or localized, solitonic behaviour emerged. For large values of l they found periodic motion, while for intermediate values of l they found various amounts of solitonic behaviour, the pulse sometimes undergoing several turns in the chain of blocks before decaying.

It is important to note that chaotic behaviour and localized events found in the studies mentioned here consider a BK model under a different, nonlinear friction law (i.e. velocity weakening). Because we find similar behaviour with the rate-and-state friction law, it introduces the question of whether or not the specific form of the friction law matters, or if the non-linearity of the law alone is sufficient in generating these dynamics.

1.4 Modelling challenges

Although the use of rate-and-state dependent friction is justified by empirical studies in the laboratory, there are disadvantages because of the difficulties that the non-linearity of rate-and-state friction imposes in the numerical simulations. As detailed in Erickson *et al.* (2008), rate-and-state friction attached to dynamic models can result in differential equations that are very stiff in the numerical sense. Naïve methods to numerically integrate these equations are extremely inefficient and computationally expensive. Lapusta & Rice (2003) incorporated a regularized formulation of rate-and-state friction in a 2-D antiplane framework. However, for the parameter range they considered, they found only periodic behaviour in their solutions. It is possible that an insufficient exploration of parameter values may be one explanation as to why chaotic regimes have rarely been observed with rate-and-state friction laws.

In addition to numerical difficulties, implementing a robust friction law in the dynamic model of an earthquake presents another fundamental challenge. Friction laws like rate-and-state, or the Free Volume law (Daub & Carlson 2008) have been developed to describe the physical processes of small samples in laboratory experiments with microscale lengths on the order of the centimetre or less. Applications of these friction laws into numerical models of earthquakes will thus require making assumptions about the spatial properties of the parameters of the friction law as current numerical implementation of a dynamic model of an earthquake requires a description of the initial stress and the friction law at a length scale of the order of ~100 m. It is possible that the emergent behaviour from a full-scale rupture model can be lost or altered when considering models of this size, as modern computing capabilities prevent us from being able to prescribe frictional properties at the microscales in a full-scale model.

In addition to possible problems introduced by attaching laboratory derived friction laws to full scale models, dynamic modelling requires a correct description of the spatio-temporal variability of parameters involved in the earthquake rupture process. This makes the simulation of the propagation of the rupture and prediction of the ground motion possible. Unfortunately there has been little agreement on proper parameter values and our evidence to date suggests that a proper quantification of parameter values across the fault is neither achieved, nor well understood. For instance, the selection of the parameters values can be complicated when heating and pore pressure are included (Rice 2006). More generally, the proper question is to determine the spatial distribution of these parameters along the fault surface. Direct estimates of them into realistic conditions prevailing during an earthquake is currently unattainable and there is no evidence that indirect estimate of the parameters of the friction laws through inversion methods will lead to an important breakthrough. For instance, current attempts to determine the spatial variability of the slip-weakening distance D_c (a parameter common to several friction laws, including the rate-and-state friction law) are inconclusive. Zhang *et al.* (2003) for example, found difficulties in the determination of values for D_c due to constraints in kinematic inversion and were able to estimate only an upper bound on values of D_c. Using a slip weakening friction law to compute the parameters of a dynamic rupture model, Peyrat *et al.* (2004) conclude, 'it may not be possible to separate strength drop and D_c using rupture modelling with current bandwidth limitations'. Using dynamic rupture inversion of a synthetic earthquake to compute the initial stress and D_c, Corish *et al.* (2007) can only estimate the average value of D_c. Furthermore, they conclude that 'there is a trade-off between the average initial stress on the fault and the slip-weakening distance that precludes identification of the exact values of either quantity based on strong-motion records'.

Although there lacks a strong consensus made for a proper regime of relevant parameter values, we develop the proper numerical methods capable of handling the numerical challenges introduced by the non-linearity of rate-and-state friction and are able to explore the parameter space quite deeply. This allows us to study the Burridge–Knopoff spring and block model subject to this friction law and analyse how each parameter influences the emergent behaviour. This in turn sheds light on the parameter values capable of reproducing earthquake dynamics and may lead to a method for determining appropriate values to be used in future dynamic rupture simulations with more sophisticated models.

2 THE 1-D DISCRETE MODEL

2.1 Extension of the single-block case

In Erickson *et al.* (2008) we conducted an in-depth study of the parameters associated with a BK model of single spring-block subject to rate-and-state friction and discussed its ability to capture 1-D earthquake motion. We began numerical simulations of the model by using the version proposed by Madariaga (1998) of a single spring-block slider. In this form one can view the block's slip relative to the pulling force or driver plate moving at v_p. Setting $v_p = v_o$ (the reference velocity in rate-and-state friction), the equations of motion (slightly modified version than those given in Erickson *et al.* 2008) coupled with 'slip-law' formulation of rate-and-state friction (eq. 1) are given by

$$\left.\begin{aligned} \dot{u} &= v - v_0 \\ \dot{v} &= (-1/M)(ku + \sigma_n\,[f^* + \Theta + a\ln(v/v_o)]) \\ \dot{\Theta} &= -(v/D_c)(\Theta + b\ln(v/v_o)) \end{aligned}\right\} \quad (4)$$

where the variables u and v correspond to the slip (relative to the driver plate) and slip velocity. Here (and from this point on) we use the large Θ notation, where $\Theta = b\ln(\frac{v_0\theta}{D_c})$ and can be interpreted as the change in interface strength from the reference friction f^* (Nakatini 2001). (This notation is more convenient and equivalent to writing it in terms of the state variable θ in eq. 1). The parameter M is the mass of the block, σ_n is the normal stress, the parameters f^*, D_c, a and b are the parameters of the rate-and-state friction law described in Section 1.2, and k is the spring stiffness. When compared to the 1-D equations of motion for an elastic layer of thickness H and shear modulus G resting on a rigid substrate, a quasi-static approximation reduces the problem to that of a spring-block model with spring stiffness given by G/H (Putelat *et al.* 2008). In this context therefore, the spring stiffness k can be considered as corresponding to the linear elastic properties of the medium surrounding the fault (Scholz 2002). System (4) can be non-dimensionalized (see Erickson *et al.* 2008, for details) into the following form

$$\left.\begin{aligned} \dot{\bar{u}} &= \bar{v} - 1 \\ \dot{\bar{v}} &= -\gamma^2[\bar{u} + (1/\xi)(\bar{f} + \bar{\Theta} + \ln(\bar{v}))] \\ \dot{\bar{\Theta}} &= -\bar{v}(\bar{\Theta} + (1+\epsilon)\ln(\bar{v})) \end{aligned}\right\} \quad (5)$$

where $\bar{u}$ is now the non-dimensional slip of the block relative to the driver plate, $\bar{v}$ is the non-dimensional slip velocity and $\bar{\Theta} = \Theta/a$ is just a scaled value of the already non-dimensional strength. The four internal parameters are

$$\gamma = \sqrt{k/M}(D_c/v_o),$$

the non-dimensional frequency,

$$\xi = (kD_c)/A,$$

the non-dimensional spring constant,

$$\epsilon = (B - A)/A$$

measures the sensitivity of the velocity relaxation and is a ratio of the stress parameters in the rate-and-state friction law and

$$\bar{f} = f^*/a$$

is the scaled steady-state friction coefficient. Although more information on A and B can be found in Section 1.2 and in Scholz (2002), the analogy with earthquake motion is that the parameter ϵ is determined by the ratio of the amount of stress dropped during an earthquake to the stress increase that accompanies a sudden change in fault velocity (see Fig. 1). Furthermore, this ratio implies that $\epsilon = 1/S$, where S is the non-dimensional seismic ratio (Andrews 1976). That a relationship between ϵ and S exists is important in light of the fact that an increase in ϵ (equivalent to a decrease in S) instigates a transition into chaotic behaviour. We found that when varying the parameter ϵ in the single spring-block model under rate-and-state friction causes the stationary state to undergo a Hopf bifurcation into a periodic orbit. After ϵ is further increased, the system period doubles into periodic orbits of 2, 4, 8, etc. After this period doubling cascade, the system reaches a chaotic state for critical values ϵ. Assuming that the friction law is responsible for the non-periodic behaviour of earthquake events (like the conclusions made by Carlson & Langer 1989), then dynamic modelling requires that ϵ be in this chaotic regime.

In the case of a single block subject to rate-and-state friction, critical values of ϵ were quite large ($\approx$11). Thus we extend this study to the case of many blocks, to see if chaos ensues for a wider parameter range including smaller values of ϵ. This information may give us insight into which features of this particular friction law are preserved, lost or added when considering systems of larger size.

We begin by deriving the discrete formulation of the Burridge–Knopoff spring-block model subject to the slip law formulation of rate-and-state friction. We find however, that in keeping ϵ fixed at the small value of 0.5, the discrete system (ODEs) exhibits both periodic and chaotic motion, where the system's transition to chaos is size-dependent, that is, how many blocks are considered. The chain undergoes periodic motion when less than 20 blocks are considered. Under the same system parameters however, the chain will undergo chaotic motion when 20 or more blocks are incorporated, although this transition depends on the parameters under consideration.

2.2 Equations of motion

The following equations of motion are derived from a 1-D chain of spring-connected blocks elastically coupled and driven by a plate moving at a constant rate v_p. The blocks slide along a rough surface according to the slip law formulation of rate-and-state friction (see Fig. 2) and the equations of motion for the jth block's position x_j are given by

$$\left.\begin{aligned} m\ddot{x}_j &= \mu(x_{j+1} - 2x_j + x_{j-1}) - \lambda(x_j - v_p t) - F_j(\dot{x}_j, \Theta_j)\\ F_j(\dot{x}_j, \theta_j) &= \sigma_n\left[f^* + \Theta_j + a\ln(\dot{x}_j/v_o)\right]\\ \dot{\Theta}_j &= -(\dot{x}_j/D_c)(\Theta_j + b\ln(\dot{x}_j/v_o)) \end{aligned}\right\}, \tag{6}$$

where F_j is the rate-and-state friction law from eq. (1), μ is the spring constant coupling the blocks, λ is the spring constant coupling each block to the driver plate, and v_0, a, b and D_c are the associated frictional parameters, described in Section 1.2. The spring constants μ and λ can be interpreted as the elastic properties across the medium (see Section 2.1), x_j is the position of the jth block, or its slip from its initial starting position.

With the simplification made by setting $v_p = v_o$, the variable x_j has two components: $x_j = u_j + v_o t$ where u_j is the block's slip relative to the driving plate, and $v_o t$ is the distance the plate has moved in t units of time. For our purposes, we rewrite the equations in terms of the variable u_j, the jth block's slip from its adjacent point on the driver plate, resulting in the following equations

$$\left.\begin{aligned} m\ddot{u}_j &= \mu(u_{j+1} - 2u_j + u_{j-1}) - \lambda u_j - F_j(\dot{u}_j, \Theta_j)\\ F_j(\dot{u}_j, \Theta_j) &= \sigma_n\left[f^* + \Theta_j + a\ln\left(\tfrac{\dot{u}_j}{v_o} + 1\right)\right]\\ \dot{\Theta}_j &= -((\dot{u}_j + v_o)/D_c)\left(\Theta_j + b\ln\left(\tfrac{\dot{u}_j}{v_o} + 1\right)\right) \end{aligned}\right\}, \tag{7}$$

where u_j is now the jth block's slip relative to the driver plate.

We non-dimensionalize the system in the manner of Madariaga (1998) [as described in Erickson *et al.* (2008)] in terms of non-dimensional variables given by $u_j = L\bar{u}_j$, $\dot{u}_j = v_o\dot{\bar{u}}_j$ and $t = \frac{L}{v_o}\bar{t}$. Θ is already non-dimensional but scaled by the value a to simplify the equations: $\Theta = a\bar{\Theta}$. The non-dimensional equations are given by

$$\left.\begin{aligned} \ddot{\bar{u}}_j &= \gamma_\mu^2(\bar{u}_{j-1} - 2\bar{u}_j + \bar{u}_{j+1}) - \gamma_\lambda^2\bar{u}_j\\ &\quad - \left(\gamma_\mu^2/\xi\right)(\bar{f} + \bar{\Theta}_j + \ln(\dot{\bar{u}}_j + 1))\\ \dot{\bar{\Theta}}_j &= -(\dot{\bar{u}}_j + 1)(\bar{\Theta}_j + (1+\epsilon)\ln(\dot{\bar{u}}_j + 1)) \end{aligned}\right\}, \tag{8}$$

where $\bar{u}_j$ is the non-dimensional slip of the jth block relative to the driver plate,

$\gamma_\mu = \sqrt{\mu/m}(D_c/v_o)$

and

$\gamma_\lambda = \sqrt{\lambda/m}(D_c/v_o)$

are the non-dimensional frequencies (the subscripts on γ are to remind the reader which spring constant they refer to—see Fig. 2),

$\xi = (\mu D_c)/A$

is the non-dimensional spring constant,

$\bar{f} = \dfrac{f^*}{a}$

is the scaled steady-state friction coefficient, and

$\epsilon = (B - A)/A$

as before (see Sections 1.2 and 2.1 for more information on ϵ, A and B).

2.3 Numerical methods

Because of the non-linearity imposed on eq. (8) by the logarithmic term from rate-and-state friction, analytic integration cannot be done even in the simplest case of a single block. For this reason, we proceed by implementing a numerical method by first writing (8) as a system of 3 first-order ODEs

$$\left.\begin{aligned} \dot{\bar{u}}_j &= \bar{v}_j\\ \dot{\bar{v}}_j &= \gamma_\mu^2(\bar{u}_{j-1} - 2\bar{u}_j + \bar{u}_{j+1}) - \gamma_\lambda^2\bar{u}_j\\ &\quad - \left(\gamma_\mu^2/\xi\right)(\bar{f} + \bar{\Theta}_j + \ln(\bar{v}_j + 1))\\ \dot{\bar{\Theta}}_j &= -(\bar{v}_j + 1)(\bar{\Theta}_j + (1+\epsilon)\ln(\bar{v}_j + 1)) \end{aligned}\right\}. \tag{9}$$

As mentioned in the previous section, rate-and-state friction has introduced numerical challenges because the non-linearity of the logarithmic term causes the system's local Jacobian matrix to possess very large negative eigenvalues—a property that usually indicates the presence of numerical stiffness (well documented in Erickson *et al.* 2008; Noda *et al.* 2009; Rojas *et al.* 2009). During our simulations conducted in Erickson *et al.* (2008) we found that even with the use of an implicit numerical method suited for numerically stiff problems, the time step was still restricted by accuracy requirements. Even with a stable method, if the time step taken is too large, then the algorithm returns numerical value of $\bar{v}_j < -1$ and the logarithmic term is undefined. For this reason, we use an embedded fourth order explicit Runge–Kutta method on the ODEs in eq. (9) whose step size adapts according to accuracy requirements.

N blocks are evenly spaced on a chain of length 20 dimensionless spatial units. Since fault rupture is caused by small stress instabilities along the fault surface and often propagate like a localized pulse (Heaton 1990), we choose to represent the initial data as localized departure from the equilibrium (or stationary) regime. The equilibrium regime is where the relative displacement $\bar{u}_j$ is constant for all j and $\bar{v}_j = \bar{\Theta}_j = 0$. Thus the equilibrium solution is $\bar{u}_j = -\frac{\bar{f}\gamma_\mu^2}{\xi\gamma_\lambda^2}$, a constant value we denote by $\bar{u}_o$. Therefore the initial data is given as departure from this state by a smooth Gaussian pulse centred at the middle block

$$\bar{u}_j(0) = \bar{u}_o + e^{\frac{-(\bar{x}_j - 10)^2}{\sigma^2}}, \quad \bar{x}_j = j(20/N)$$

$$\text{for } j = 1, \ldots N, \text{ where } \sigma = 1,$$

$$\bar{v}_j(0) = 0, \quad \text{for } j = 1, \ldots N$$

Since $\bar{u}_o$ is negative, the chain's equilibrium solution is behind the driver plate. The Gaussian pulse corresponds to imposing an initial stress perturbation in the initial position of each block from this equilibrium position, the middle block having the greatest perturbation. All have zero initial velocity (with respect to the driver plate). Free boundary conditions imply that blocks on either end of the chain are only influenced by the single block connecting them to the chain, and their elastic coupling with the driver plate.

2.4 Transition to chaos

Because of a lack of insight into proper parameter values (explained in Section 1.4), we explore the parameter space that allows for more manageable numerical computation (i.e. where the parameters associated with the non-linear terms are not too large). Numerical integration is done for different amounts of blocks: $N = 3$, 9 and 20 blocks. Parameter values used here are fixed at $\gamma_\mu = 0.5$, $\gamma_\lambda = \sqrt{0.2}$, $\xi = 0.5$, $\epsilon = 0.5$ and $\bar{f} = 3.2$. Figs 3, 4 and 5 correspond to different amounts of blocks considered. For each figure, plot (a) is

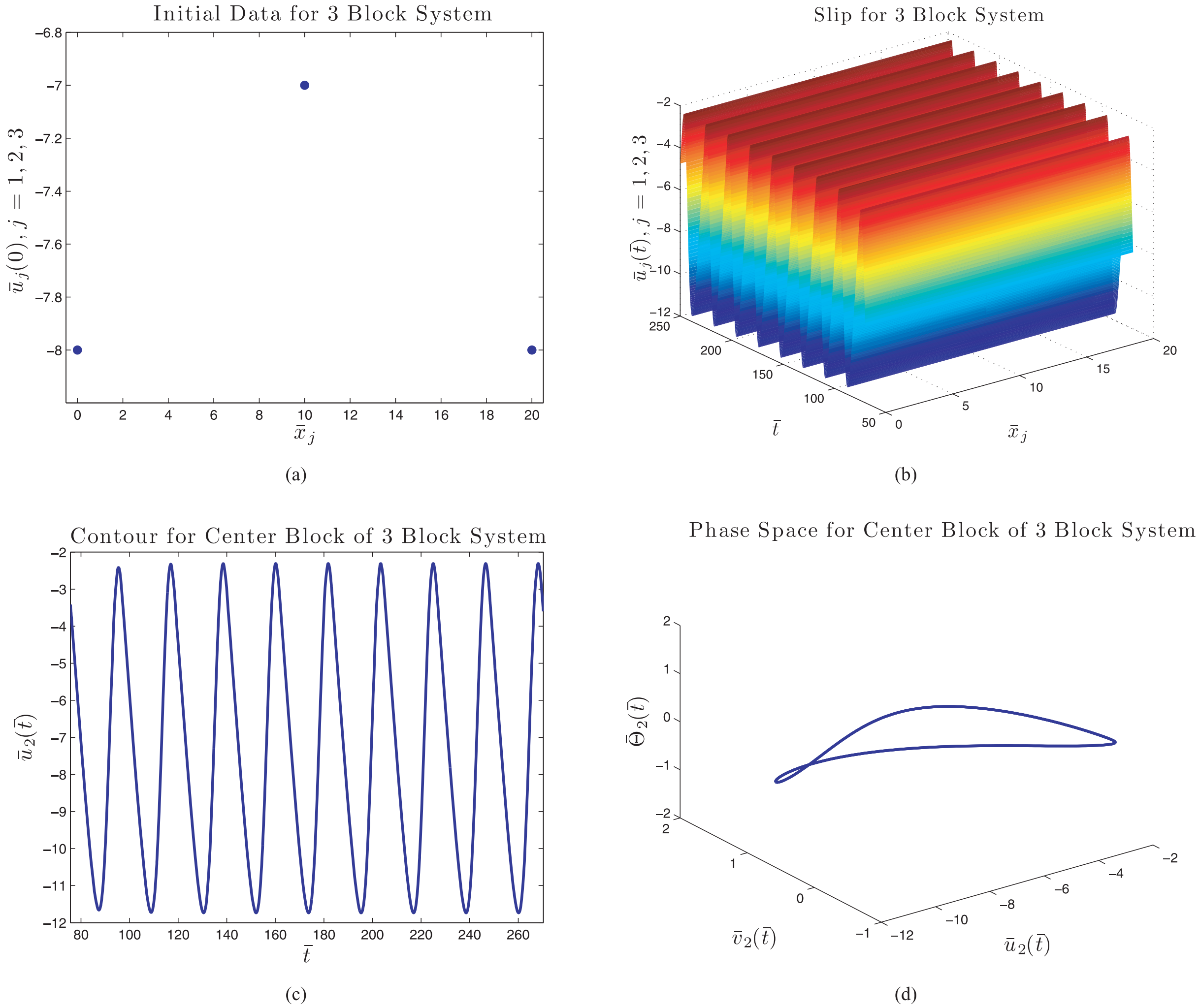

Figure 3. Solution to the ODEs (9) derived from a three block system with parameter values $\epsilon = 0.5$, $\xi = 0.5$, $\gamma_\mu = 0.5$, $\gamma_\lambda = \sqrt{0.2}$ and $\bar{f} = 3.2$. (a) Initial data, where the Gaussian perturbation from equilibrium only affects the middle block. (b) Slip of all three blocks against time where the motion is periodic in time, each block attaining the same amplitude. Negative values in relative slip correspond to the chain's position being behind the driver plate, and slipping almost to the point adjacent to the driver plate (where the relative slip would then be zero). (c) Slip of the middle block against time, where an initial transient period exists during which the small instabilities introduced by the initial slip perturbation are amplified, then saturated by the system's non-linearities and then settle into periodic motion. (d) Middle block's slip, velocity and state variable value in the phase space. Plots (c) and (d) emphasize the periodic motion that this block undergoes.

the initial displacement of all N blocks and (b) is the slip of all N blocks against time. Negative values in relative slip correspond to the block's position being behind the driver plate, while a relative slip value close to zero corresponds to slipping almost to the point adjacent to the driver plate. Plot (c) in Figs 3–5 is the contour of the middle block's slip against time and one can further view the periodic or chaotic behaviour emerging, while plot (d) is the phase space for the middle block's slip, velocity and state variable. Periodic orbits will appear as a single closed loop in the phase space, while chaotic orbits will appear as a strange attractor (see Erickson *et al.* 2008, for more explanation).

Fig. 3 shows the results from a system of three connected blocks. After a transient period in which the initial perturbation is amplified, the non-linearities saturate this growth and the system settles into the same periodic trajectory—suggesting that the blocks move collectively. All three blocks undergo abrupt, periodic motion of period approximately 20 temporal units and relative amplitude approximately four slip units. Recall that these non-dimensional time and space variables are scaled by D_c/v_o and D_c (respectively). The blocks are stuck to the rough surface (thus the relative displacement decreases) until the driver plate overcomes the static friction holding each block in place, and the chain suddenly begins to slide. The blocks slide forward, approaching their adjacent point to the driver plate before slowing down due to frictional resistance. The driver plate then moves beyond the chain and once the pulling force overcomes static friction, the cycle begins again. Sudden and jerky motion, reminiscent of stick-slip behaviour emerges as the blocks respond to the driver plate. Under the same parameter combination however, periodic motion occurs when considering the system of nine blocks as viewed in Fig. 4, although it appears that the period of the solution has undergone at least one period doubling bifurcation. In this case all nine blocks undergo periodic motion, but their slip values reach different amplitudes—the blocks near the centre of the chain do not slide as far as those near the end of the chain.

For this fixed set of parameter values, the resulting motion suggests periodic behaviour for values of $N < 20$. For $N = 20$ however, the motion becomes chaotic. As seen in Fig. 5, each block follows

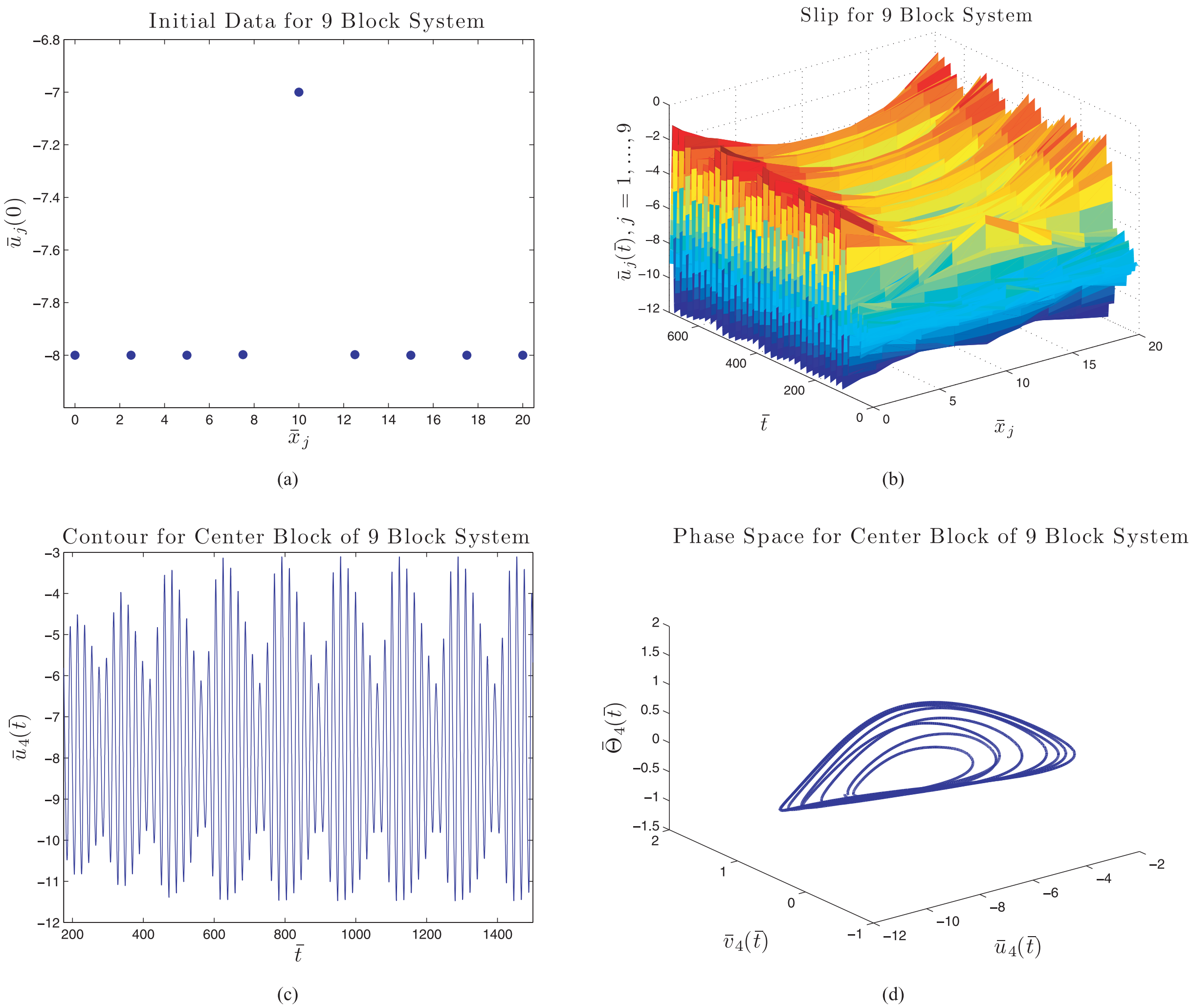

Figure 4. Solution to the ODEs (9) derived from a 9 block system with parameter values $\epsilon = 0.5$, $\xi = 0.5$, $\gamma_\mu = 0.5$, $\gamma_\lambda = \sqrt{0.2}$ and $\bar{f} = 3.2$. (a) Initial data, where the blocks are given an initial perturbation from equilibrium in the form of a smooth Gaussian pulse. (b) Slip of all nine blocks against time where after a transient period, the chain settles into what appears to be periodic motion. Negative values in relative slip correspond to the chain's position being behind the driver plate, and slipping almost to the point adjacent to the driver plate (where the relative slip would then be zero). The blocks reach different amplitudes, the centre block and blocks near the end reaching an amplitude of about three units, while the remaining blocks reach smaller amplitudes. (c) Slip of the centre (fourth) block against time, where an initial transient period exists during which the small instabilities introduced by the initial slip perturbation are amplified, then saturated by the system's non-linearities and then settle into periodic motion. (d) Centre block's slip, velocity and state variable value in the phase space. Plots (c) and (d) emphasize the periodic motion that this block undergoes.

its own chaotic trajectory in time and the blocks appear to move independently of each other—suggesting chaotic behaviour in space as well. Further studies show that this transition to chaotic motion varies, depending on the parameters considered. More specifically, the fact that chaotic behaviour emerges at $N = 20$ is not universal; it depends on the parameters used. It is also important to note that regardless of the type of motion these systems produce, one can observe from Figs 3–5 that there is a transient period during which small instabilities introduced by the initial slip perturbation are amplified as energy enters the system. This amplification is then saturated by the non-linearities present from the friction law. This feature suggests that under these parameter values, the friction law can be a mechanism responsible for causing even small instabilities to grow into large, but finite events, similar to the conclusions made by Carlson & Langer (1989) who stated that the velocity weakening friction law was responsible for the amplification of small heterogeneities in the initial spatial distribution, leading to chaotic motion.

Further insight into these solutions is gained by computing the Fourier power spectrum [see (Erickson *et al.* 2008) for details on how the power spectrum is computed] as viewed in Fig. 6. We consider the middle block in each chain of length 3, 9 and 20 blocks. Fig. 6 shows the power spectrum normalized with respect to the fundamental frequency (frequency with the most power) for the system of 3, 9 and 20 blocks, and one can further view the periodic or chaotic motion of these systems. Fig. 6(a) is the power spectrum for three blocks showing its power concentrated at the dominant frequency and at one harmonic, suggesting that the solution has period 2 (although visibly it appears to have period 1). Fig. 6(b) shows the power spectrum (and corresponding zoom) for nine blocks where there appears approximately eight peaks, suggesting periodic behaviour with period 8. Fig. 6(c) shows the power spectrum for the system of 20 blocks, where broad-band noise is present, suggesting chaotic motion.

We can view the chaotic behaviour in the power spectrum in more detail by plotting the log–log plot of the power against the

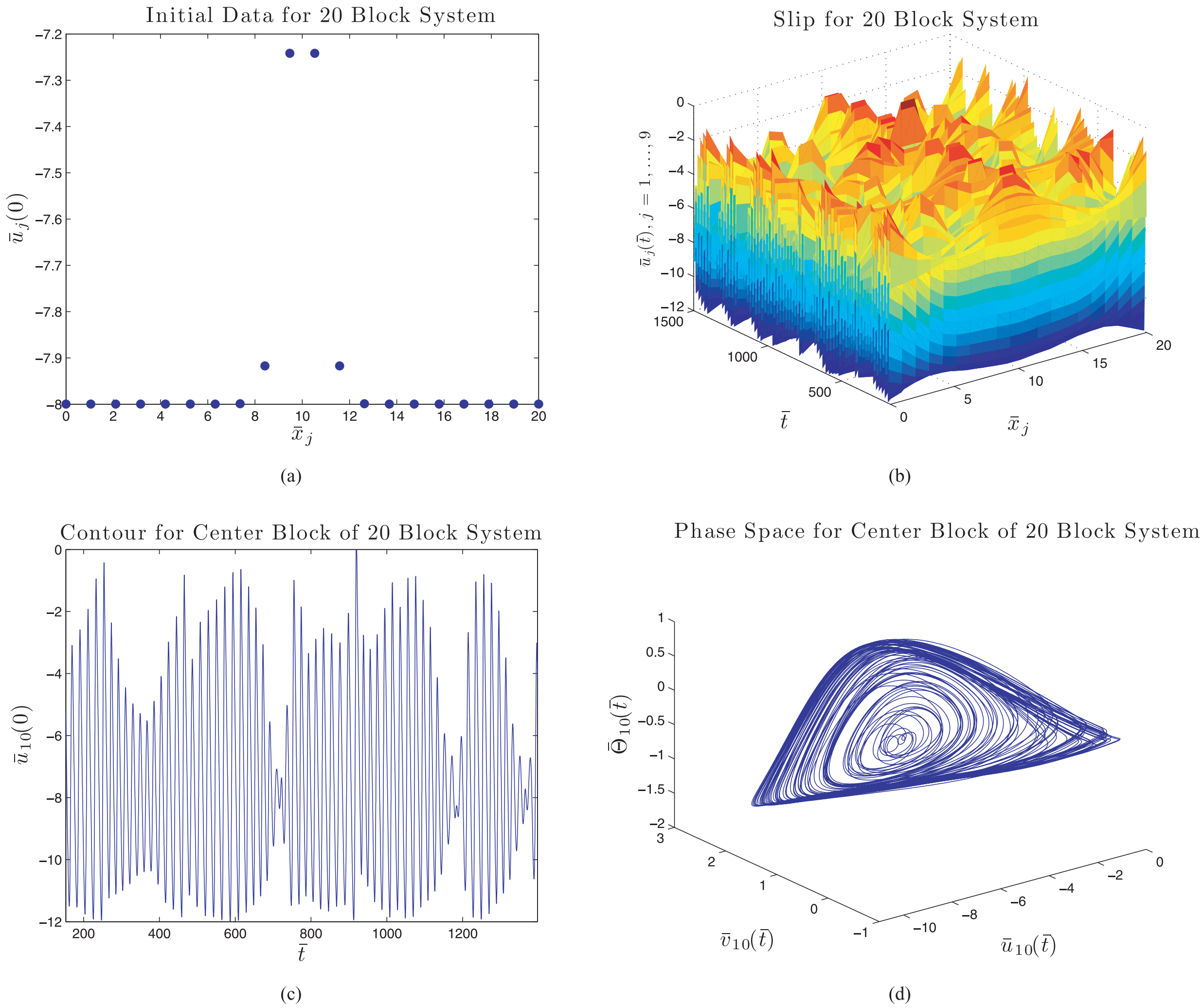

Figure 5. Solution to the ODEs (9) derived from a 20 block system with parameter values $\epsilon = 0.5$, $\xi = 0.5$, $\gamma_\mu = 0.5$, $\gamma_\lambda = \sqrt{0.2}$ and $\bar{f} = 3.2$. (a) Initial data, where the blocks are given an initial perturbation from equilibrium in the form of a smooth Gaussian pulse. (b) Slip of all 20 blocks against time maintaining what appears to be chaotic motion. Negative values in relative slip correspond to the chain's position being behind the driver plate, and slipping almost to the point adjacent to the driver plate (where the relative slip would then be zero). (c) Slip of the centre (tenth) block against time, where an initial transient period exists during which the small instabilities introduced by the initial slip perturbation are amplified, then saturated by the system's non-linearities and undergo chaotic motion. (d) Centre block's slip, velocity and state variable value in the phase space. Plots (c) and (d) emphasize the chaotic motion that this block undergoes.

frequency. Fig. 6(d) shows this data for the chaotic solution from the 20 block system. We see that the spectra for this system experiences two regimes of decay. There is an initial period where the power spectrum undergoes exponential decay (at least qualitatively), before converging to a line and undergoing a slower, algebraic (power-law) decay. Sigeti (1995) acknowledges the common agreement that the power spectra computed from continuous-time dynamic systems within the chaotic regime experience exponential decay. That this is followed by a second regime in which a power-law behaviour is present has also been seen in several dynamic systems that exhibit chaos, like those documented in Valsakumar *et al.* (1997). The power-law behaviour is a feature not uncommon to many areas of geology and geophysics and evidence of a fractal distribution [see (Turcotte 1997) and references therein]. For instance, the well known Gutenberg–Richter law for frequency–magnitude earthquake distribution follows a power law, as does topography (Turcotte 1997) and turbulent flow (Frisch 1995).

So far these results only suggest a transition to chaos, but a true signature of chaotic behaviour is the existence of a positive Lyapunov exponent. The idea is to quantify the rate of divergence under the flow of two close by trajectories (sensitive dependence on initial data), see Verhulst (2000) and Sandri (1996), among others, for a more detailed explanation. For a continuous dynamical system like that given by eq. (9), the linearized equations governing the evolution of a perturbation $\boldsymbol{\delta}$ are given by the variational equations

$$\dot{\boldsymbol{\delta}} = \boldsymbol{J}(t, \mathbf{y})\boldsymbol{\delta}, \tag{10}$$

where $\boldsymbol{J}(t, \mathbf{y})$ is the Jacobian matrix defined by the right side of eq. (9). The variational equations are solved simultaneously with eq. (9) and the maximal Lyapunov exponent is given by the following limit (Oseledec 1968)

$$\lim_{t\to\infty} \frac{1}{t} \ln \|\boldsymbol{\delta}(t)\|$$

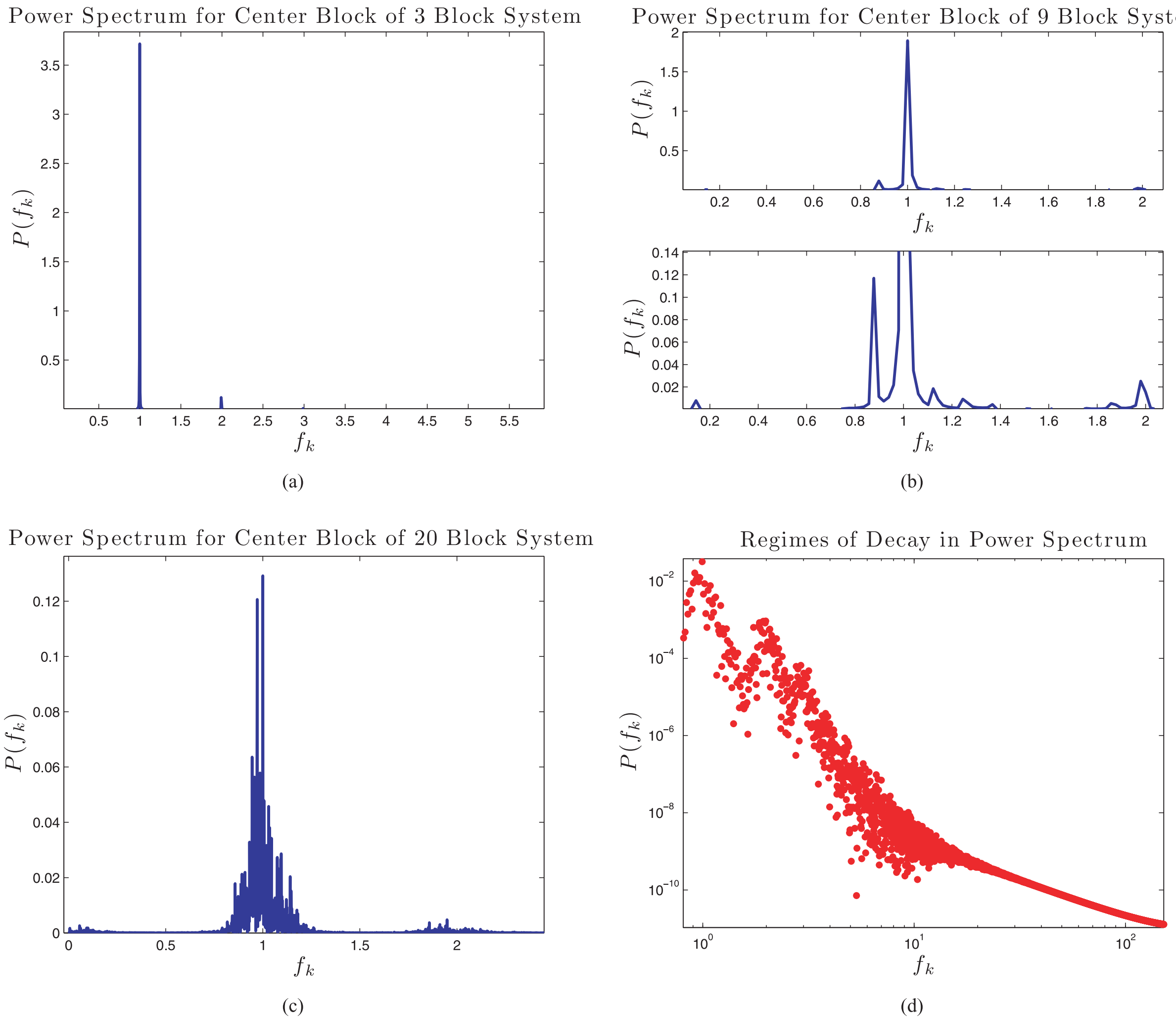

Figure 6. Normalized power spectra for the slip associated for (a) 3 blocks, (b) 9 blocks and (c) 20 blocks. (a) and (b) further emphasize the periodic behaviour of the solutions to the model when considering 3 and 9 blocks. Both plots reveal a finite amount of peaks, with 1 or 2 strong peaks and several harmonics. (c) Normalized power spectra for the slip associated with 20 blocks where a transition to chaos occurs, as broad-band noise is evidenced by the high number of frequencies represented. (d) Log–log plot for power against frequency for the system of 20 blocks shows two regimes of decay. We see an initial period where the power spectrum experiences (qualitatively) exponential decay, but this is followed by slower, algebraic (power-law) decay.

Numerical calculations of the maximal Lyapunov exponent for the dynamic system given by eq. (9) for the discrete system of $N = 3$ and 9 blocks show that the maximal Lyapunov exponent decays towards zero (thus periodic motion). Fig. 7 however, shows this exponent for the system of 20 blocks and it is clear that it approaches a small but positive value, implying chaotic motion.

3 THE CONTINUUM FORMULATION

3.1 Extension of the discrete model

As we have seen in the previous section, chaotic dynamics emerge in the discrete formulation when the number of blocks is increased. For this reason, we are interested in studying the dynamics of a continuum model to see if the behaviour undergoes qualitative changes when considering infinitely many blocks. In this section, we derive the non-linear wave equation from the Burridge–Knopoff spring block system subject to the rate-and-state friction law. We find that a transition to chaos also occurs when varying the parameter ϵ, similar to what we found in Erickson *et al.* (2008) for the case of a single block. The critical value of ϵ however, is much smaller than that required for a single block.

3.2 Equations of motion

Going back to the dimensional ODEs given by eq. (7), we can derive a continuous model for a chain of infinitely many blocks by taking the continuum limit in the manner similar to Carlson & Langer (1989) who considered the equilibrium spacing between the blocks (denoted here by Δx). Taking $\Delta x \to 0$ and $m \to 0$ (the mass of each block) derives a partial differential equation (PDE), where the spring coefficient between blocks gets stiffer ($\mu \sim \frac{1}{\Delta x}$), the spring connecting each block to the driver plate gets weaker ($\lambda \sim \Delta x$). Consequently the stress parameters $A = \sigma_n a$ and $B = \sigma_n b$ decrease like $\sim\Delta x$. In this framework the ratio $\frac{m}{\Delta x}$ is the mass per unit length of string, or linear density (Pain 1968) which is held constant. Then we consider eq. (7) and the corresponding non-dimensional eq. (8) when $\Delta x \to 0$ and $m \to 0$, with the additional rescaling: $x = D_c \bar{x}$. This yields our final equations of motion, given by the following elastic wave equation for $\bar{u}(\bar{x}, \bar{t})$ under rate-and-state friction and

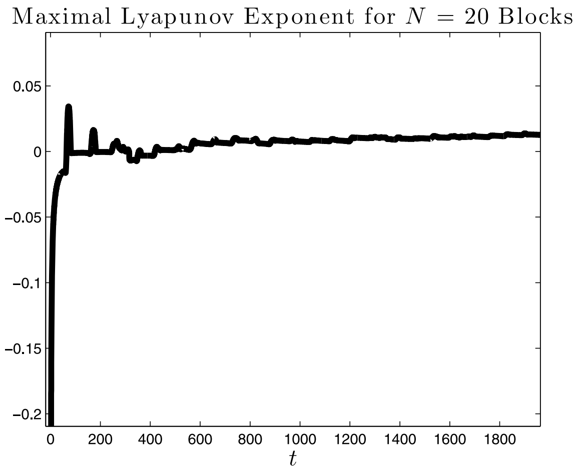

Figure 7. Maximal Lyapunov exponent for $N = 20$ blocks. A positive maximal Lyapunov exponent implies that close by trajectories diverge exponentially with a rate given by the value of the exponent. Clearly, as $t \to \infty$, the exponent approaches a small but positive value, implying that the behaviour for the system of 20 blocks is indeed chaotic.

its associated state variable evolution equation

$$\left.\begin{aligned} \frac{\partial^2\bar{u}}{\partial \bar{t}^2} &= c^2\frac{\partial^2 \bar{u}}{\partial \bar{x}^2} - \gamma_\lambda^2 \bar{u} - \left(\gamma_\mu^2/\xi\right)\left(\bar\Theta + \bar{f} + \ln\left(\frac{\partial \bar{u}}{\partial \bar{t}}+1\right)\right) \\ \frac{\partial\bar\Theta}{\partial\bar{t}} &= -\left(\frac{\partial\bar{u}}{\partial\bar{t}}+1\right)\left(\bar\Theta + (1+\epsilon)\ln\left(\frac{\partial \bar{u}}{\partial \bar{t}}+1\right)\right) \end{aligned}\right\}, \qquad (11)$$

where the final equations now involve the following finite-valued parameters

$$c^2 = \lim_{\Delta x, m\to 0}\left(\mu D_c^2 \Delta x^2\right)/\left(m v_o^2\right)$$

the square of the wave speed,

$$\frac{\gamma_\mu^2}{\xi} = \lim_{\Delta x, m\to 0}\frac{(\sqrt{\mu/m}(D_c/v_o))^2}{(\mu D_c)/A}$$

is a finite ratio of the square of the non-dimensional frequency to spring constant (as in Section 2.2),

$$\gamma_\lambda^2 = \lim_{\Delta x, m\to 0}\left(\sqrt{\lambda/m}(D_c/v_o)\right)^2,$$

is the square of the second non-dimensional frequency,

$$\epsilon = (B - A)/A$$

and

$$\bar{f} = \frac{f^*}{a}$$

as before.

3.3 Numerical methods

To solve eq. (11) numerically, we first write it as a system of three first-order equations in time

$$\left.\begin{aligned} \frac{\partial\bar{u}}{\partial\bar{t}} &= \bar{v} \\ \frac{\partial\bar{v}}{\partial\bar{t}} &= c^2\frac{\partial^2\bar{u}}{\partial\bar{x}^2} - \gamma_\lambda^2\bar{u} - \left(\gamma_\mu^2/\xi\right)(\bar\Theta + \bar{f} + \ln(\bar{v}+1)) \\ \frac{\partial\bar\Theta}{\partial\bar{t}} &= -(\bar{v}+1)(\bar\Theta + (1+\epsilon)\ln(\bar{v}+1)) \end{aligned}\right\}. \qquad (12)$$

We discretize the PDE using the method of lines (Ascher & Petzold 1998) and the spatial derivative $\frac{\partial^2\bar{u}}{\partial\bar{x}^2}$ is approximated using finite differences. For the linear transport equation for instance, the size of the spatial mesh is determined by the shortest wavelength (Gustafsson 2008) and with a time step taken to maintain stability, the numerical solution should converge under mesh refinement. Although it has been studied for different problems in the rate-and-state context (Rice & Ruina 1983; Rice 1993; Rice *et al.* 2001), the non-linearities in our problem make this kind of analysis very difficult. Since we have seen in previous sections that solutions to the discrete model are highly dependent on the number of blocks N, it is likely that these amounts of blocks are not sufficient to approximate the continuous PDE and so we do many grid refinements until we see little change in the numerical solution. Discretizing the interval $\bar{x} \in [0, 20]$ into $M = 200$ grid points, resulting in 200 ordinary differential equations and assign the continuous version of the same initial slip as the discrete system in Section 2 (chosen to represent localized departure from equilibrium), with zero initial velocity

$$\bar{u}(\bar{x}, 0) = \bar{u}_o + e^{\frac{-(\bar{x}-10)^2}{\sigma^2}}, \quad \text{where } \sigma = 1,$$

$$\bar{v}(\bar{x}, 0) = 0.$$

The free boundary conditions in the discrete model transfer to homogeneous Neumann boundary conditions: $\frac{\partial\bar{u}}{\partial\bar{x}}(\bar{t}, 0) = \frac{\partial\bar{u}}{\partial\bar{x}}(\bar{t}, 20) = 0$. As mentioned in the previous section, this form of the initial data was chosen to represent localized departure from the equilibrium position and corresponds to slightly displacing the centre of the continuum of blocks.

The spatial discretization yields the following system of ODEs

$$\frac{d}{dt}\begin{bmatrix} \bar{v}_0 \\ \bar{v}_1 \\ \cdot \\ \cdot \\ \bar{v}_i \\ \cdot \\ \cdot \\ \cdot \\ \bar{v}_M \end{bmatrix} = \begin{bmatrix} \tilde\beta & \alpha & & & & & & \\ \alpha & \beta & \alpha & & & & & \\ & \cdot & \cdot & \cdot & & & & \\ & & \cdot & \cdot & \cdot & & & \\ & & & \alpha & \beta & \alpha & & \\ & & & & \cdot & \cdot & \cdot & \\ & & & & & \cdot & \cdot & \cdot \\ & & & & & & \cdot & \cdot & \cdot \\ & & & & & & & \alpha & \tilde\beta \end{bmatrix}\begin{bmatrix} \bar{u}_0 \\ \bar{u}_1 \\ \cdot \\ \cdot \\ \bar{u}_i \\ \cdot \\ \cdot \\ \cdot \\ \bar{u}_M \end{bmatrix} - \frac{\gamma^2}{\xi}\begin{bmatrix} \bar\Theta_0 + \bar{f} + \log(\bar{v}_0 + 1) \\ \bar\Theta_1 + \bar{f} + \log(\bar{v}_1 + 1) \\ \cdot \\ \cdot \\ \bar\Theta_i + \bar{f} + \log(\bar{v}_i + 1) \\ \cdot \\ \cdot \\ \cdot \\ \bar\Theta_M + \bar{f} + \log(\bar{v}_M + 1) \end{bmatrix},$$

where $\alpha = \frac{c^2}{\Delta x^2}$, $\beta = -2\frac{c^2}{\Delta x^2} - \gamma_\lambda^2$, $\tilde\beta = -\frac{c^2}{\Delta x^2} - \gamma_\lambda^2$ and $M = 200$ (in this study) is the number of spatial points in the discretization. Due to such a large system of ODEs, we solved them in parallel using the embedded Runge–Kutta scheme discussed in Section 2 (for a summary of the parallel methods developed, see Erickson 2010). With the goal in mind of answering whether or not the features of the rate-and-state friction law are scale-dependent, we study the critical values of ϵ that lead to aperiodic behaviour to see if the transition to chaos occurs for smaller values.

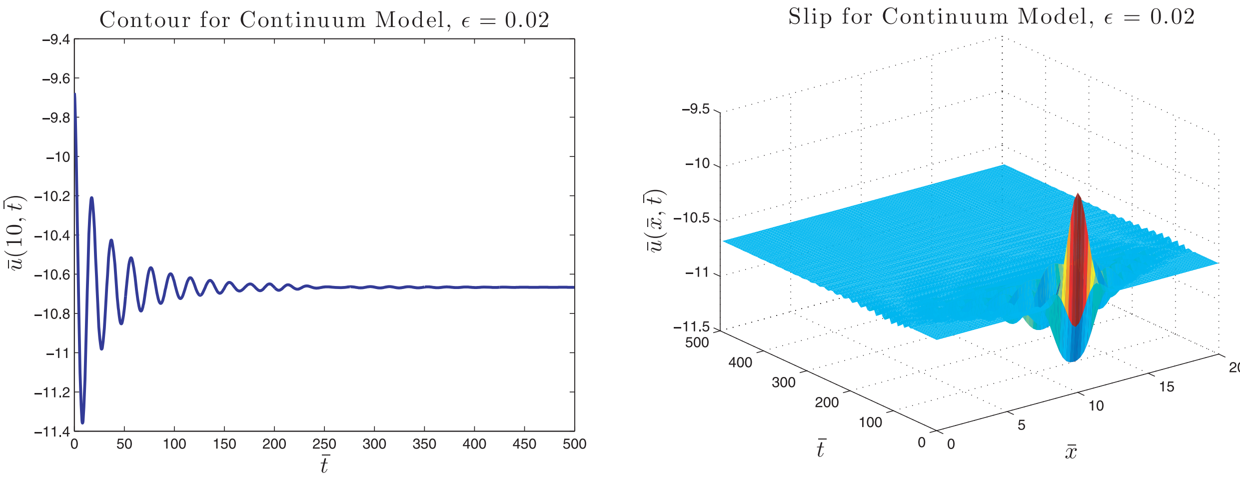

(a) (b)

Figure 8. Parameter combination $(c, \epsilon, \xi, \gamma_\mu, \gamma_\lambda) = (0.2, 0.02, 0.5, 0.5, \sqrt{0.15})$ yields a stationary solution to the PDE (12). (a) Initial data is given in the form of a Gaussian centred perturbation from equilibrium. (b) Slip of the entire chain against time. During the initial transient region, the chain is pulled forward by the driver plate. But after this time, the entire chain settles on its equilibrium position behind the driver plate, and the entire chain slides along at a constant rate with the moving plate. Thus relative slip values become constant and the relative velocity is zero.

3.4 Transition to chaos

Varying only the parameter ϵ, Fig. 8(a) shows the contour of a stationary trajectory in the centre of space ($\bar{x} = 10$) as well as the slip of the entire chain against time Fig. 8(b), while Figs 9 and 10 show plots of the initial data, the slip of the entire chain against time, the contour plot and the phase space of the trajectory in the centre of space ($\bar{x} = 10$). Parameter combination $(c, \epsilon, \xi, \gamma_\mu, \gamma_\lambda) = (0.2, 0.02, 0.5, 0.5, \sqrt{0.15})$ yields a stationary solution as seen in Fig. 8. The perturbation introduced from the initial displacement is amplified as the chain is pulled forward by the driver plate during an initial transient period. Because the friction along the surface is a function of each point's velocity $\bar{v}(\bar{x}, \bar{t})$ and state variable $\bar{\Theta}(\bar{x}, \bar{t})$, each point responds differently in how far it slips. The centre of the chain slips the greatest amount, relative to the driver plate, while the points near the ends of the chain remain almost stationary (sliding steadily with the driver plate). When the initial slip amplification is saturated by the non-linearities, each point settles on its equilibrium position $\bar{u}_o$ and the whole chain slides along at a constant rate with the moving plate.

A bifurcation of this stationary state occurs when ϵ is increased from 0.02 to 0.12, as viewed in Fig. 9 where a periodic solution emerges. After a transient period, the chain oscillates periodically, while remaining behind the driver plate and the points in the centre and the ends attain the most extreme values. The smoothness in the dynamics (see the phase space in Fig. 9d) represents a fluid-like interaction between each point along the chain and the rough surface it slides upon. The chain fluctuates in response to the driver plate and the friction on the surface, undergoing periodic cycles slowing down and then sliding forward again. For $\epsilon = 0.4$, chaotic motion appears in Fig. 10 and one can see each point along the chain undergoing its own chaotic motion as waves of different amplitudes propagate through the medium and interact with the boundary.

We can view these periodic and chaotic solutions further by computing the associated power spectra. Fig. 11(a) is associated with the periodic solution from Fig. 9, showing the normalized power spectrum and what appears to be 1 dominant frequency indicating period 1 behaviour. Fig. 11(b) is the power spectrum associated with the chaotic solution from Fig. 10 showing peaks at many frequencies. To view the power spectrum for the chaotic solution more deeply we plot the log–log plot of the power against the frequency. Fig. 11(c) shows the decay of the power spectra for the chaotic solution experiencing exponential decay (at least qualitatively) for a short time period, before converging to a line and decaying as a power law (algebraic decay). See Section 2.4 for more on this type of behaviour.

4 LOCALIZED SOLUTIONS

4.1 Solitons and breathers

During the studies conducted in Sections 2 and 3, we also observed that in certain parameter regimes both the discrete and the continuous formulations of the Burridge–Knopoff model subject to the slip law formulation of rate-and-state friction exhibit solutions where initial slip pulses remain localized in space. Like Español (1994) who studied a BK model with velocity weakening friction, we also found solutions that propagate like a travelling wave. The localized solutions suggest the presence of solitonic behaviour, where initial data in the form of a smooth Gaussian pulse tends to remain localized under certain parameter values. In the case of a travelling wave we see evidence of a soliton, a solitary wave that maintains its shape while it travels at a constant speed through the medium. The solutions that remain localized in space and oscillate in time however, are known as breathers.

The general definition of a soliton solution to a non-linear wave equation is that it has three properties: it is a wave with permanent form, that is localized in space for each fixed point in time, and if two solitons meet, their forms are preserved after the interaction (Mickens 2004). A breather, on the other hand, is a time-periodic, exponentially decaying (in space) solution of a non-linear wave equation (Kichenassamy 1991). Breather solutions are rare and the only non-linear wave equation known to possess large breather solutions is the sine-Gordon equation (see Birnir 1994; Birnir *et al.* 1994, and references therein).

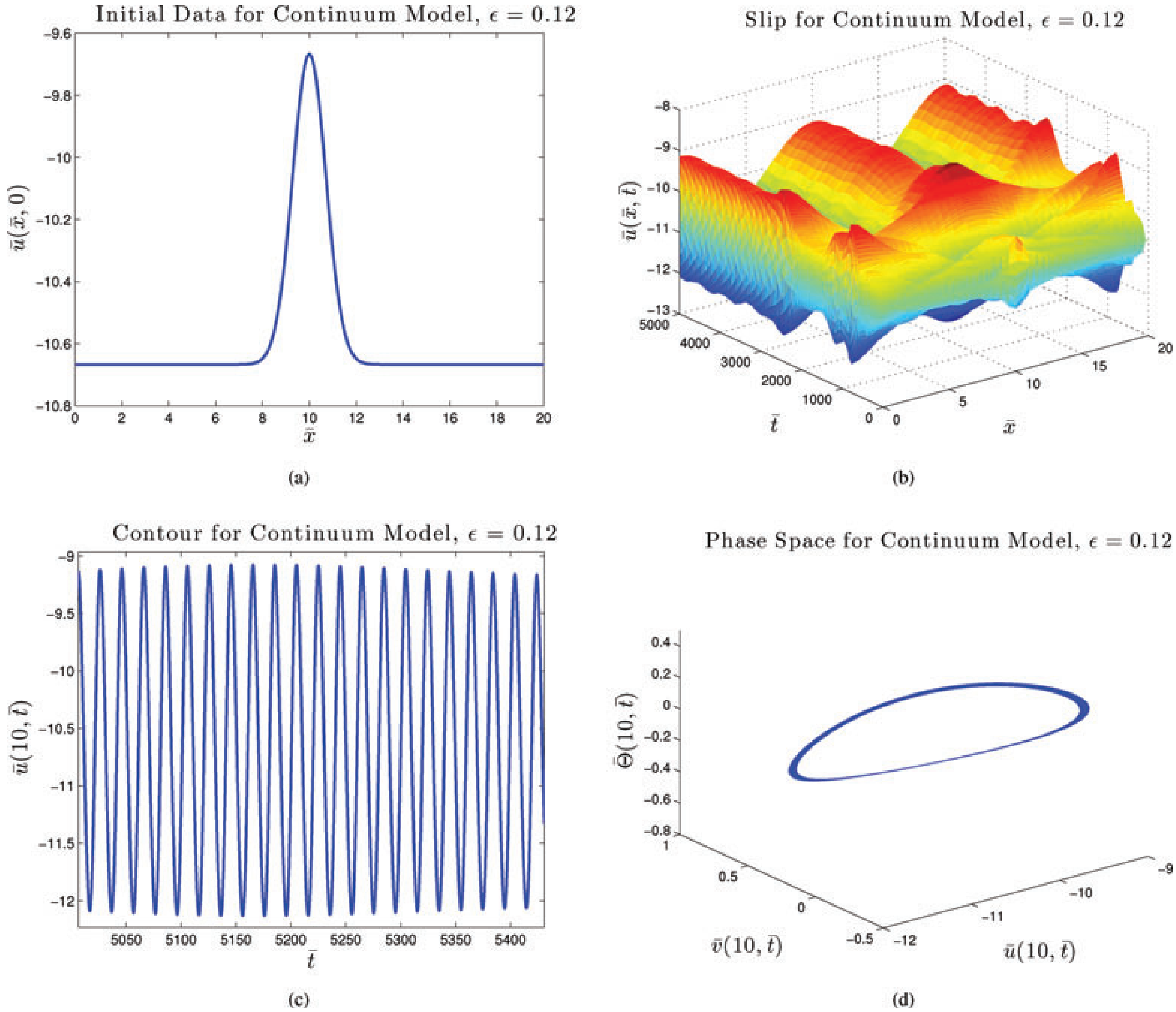

Figure 9. Parameter combination $(c, \epsilon, \xi, \gamma_\mu, \gamma_\lambda) = (0.2, 0.12, 0.5, 0.5, \sqrt{0.15})$ yields a periodic solution to the PDE in eq. (12). (a) Initial displacement is the same as in as in Fig. 8(a) we observe that an increase in ϵ from 0.02 to 0.12 yields a bifurcation of the stationary state. (b) Slip of entire system against time. During the initial transient region, the blocks are pulled forward by the driver plate, where their response to frictional resistance determines how far they slip. But after this time, each block settles on a periodic response to the driver plate, alternating between sliding and slowing down in response to the pull of the driver plate, and the roughness of the surface. (c) Contour plot of centre point on the chain and (d) phase space further suggest the periodic behaviour of the system.

4.2 Significance of localized solutions

The significance of these types of solitary wave solutions was emphasized by Heaton (1990), who studied dislocation time histories generated from models derived from earthquake waveforms. He found that, contrary to crack-like dynamic rupture models where the rise time was comparable to the entire duration of rupture along the fault, dislocation rise times were only about 10 per cent of the overall rupture duration. The most appropriate explanation for this observation of short slip durations is that the rupture travels like a self-healing pulse that propagates along the fault. Heaton suggests that a dynamic friction law (he considers a law that is inversely related to slip velocity) can be a mechanism for causing the fault to heal itself shortly after the rupture passes through, resulting in a localized pulse. The rest of this section is devoted to the exploration of the space of parameter values for which these types of soliton or breather solutions emerge for the continuum equation with the slip law form of rate-and-state friction, eq. (12). These solutions can be understood as a proxy for the propagation of the rupture front across the fault surface during an earthquake and may determine a range for suitable parameter values to be used in dynamic modelling of earthquakes.

4.3 Localized solutions to discrete and continuous formulation

As detailed in the introduction, Schmittbuhl *et al.* (1993) and Español (1994) observed (among others) solitary wave-type solutions when varying different parameters of the BK model subject to a velocity weakening friction law. Similar to the discoveries described in these papers, we have also seen solitary wave and localized solutions in both the discrete and the continuous models under the slip law formulation of the rate-and-state friction law. Figs 12 and 13 show solutions from the ODEs and the PDE under similar conditions, where solitary, localized or delocalized

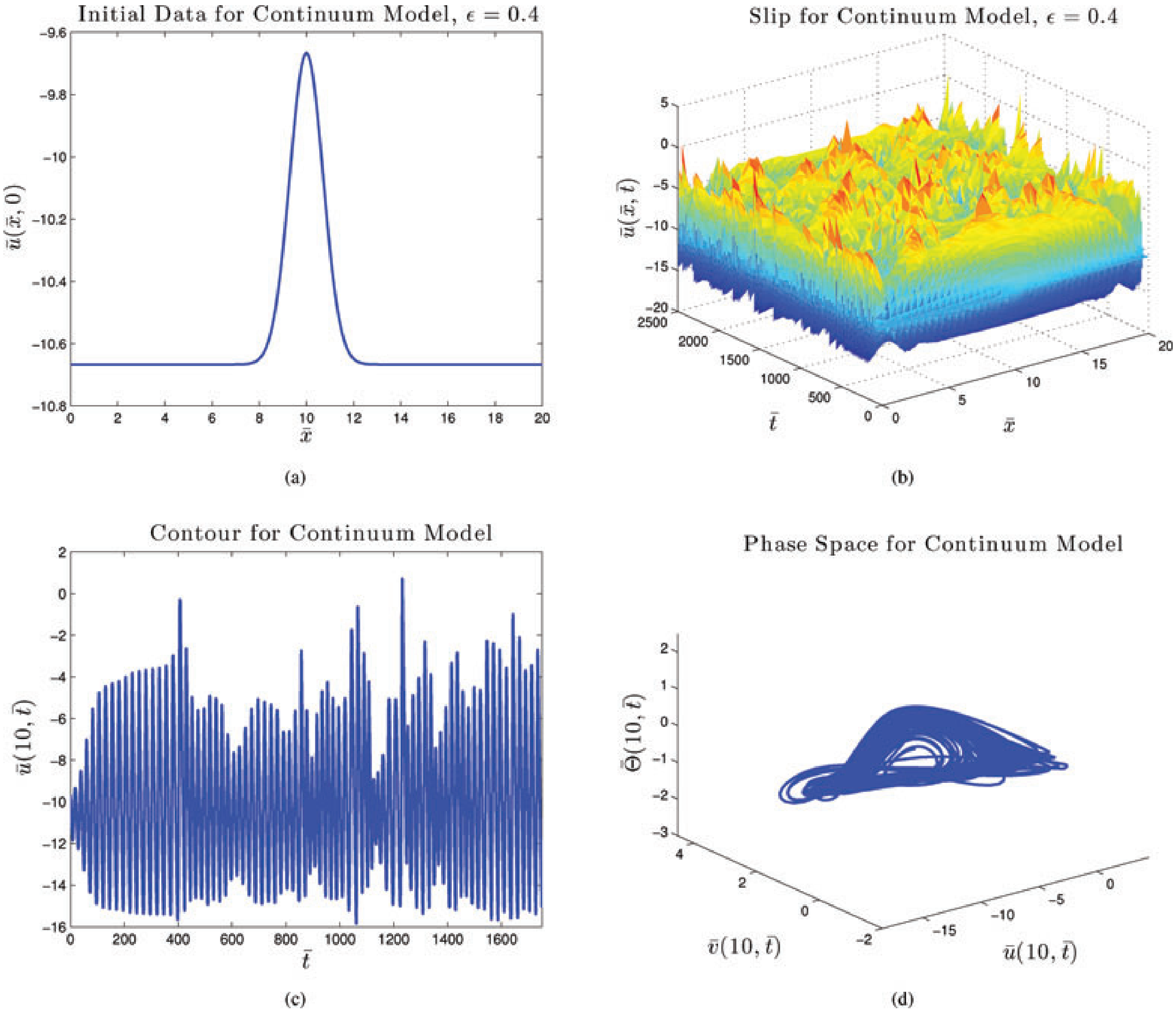

Figure 10. Parameter combination $(c, \epsilon, \xi, \gamma_\mu, \gamma_\lambda) = (0.2, 0.4, 0.5, 0.5, \sqrt{0.15})$ yields an aperiodic solution to the PDE in eq. (12). (a) Initial data is the same as before (see Figs 8a and 9b), the blocks are slightly displaced from their adjacent points on the driver plate. The parameter ϵ has been increased from 0.12 (periodic motion) to 0.4. (b) Slip of entire system against time. During the initial transient region, the blocks are pulled forward by the driver plate but respond chaotically to frictional resistance. (c) Contour plot of centre point on the chain and (d) phase space further suggest the chaotic behaviour of the system. Each point in space appears to undergo independent chaotic motion—suggesting the presence of spatial as well as temporal chaos.

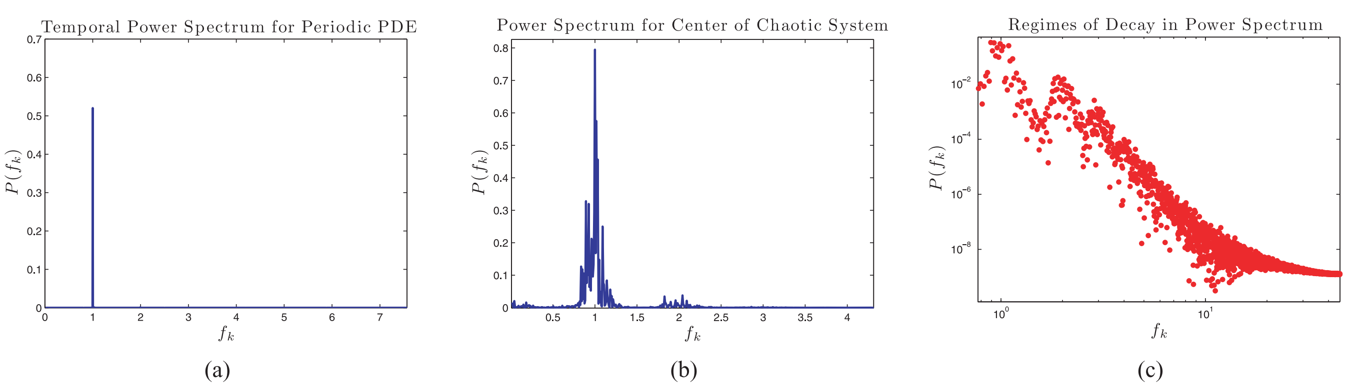

Figure 11. Normalized power spectra for periodic and aperiodic solutions to the PDE in eq. (11). (a) Power spectrum for the periodic solution shown in Fig. 9, with one dominant peak suggesting period 1 behaviour. (b) Power spectrum for the chaotic solution show in Fig. 10, showing many high peaks and clusters of harmonics. (c) Log–log plot for power against frequency for the chaotic solution to the PDE in eq. (11) shows two regimes of decay. We see an initial period where the power spectrum experiences (qualitatively) exponential decay, but this is followed by slower, algebraic (power-law) decay.

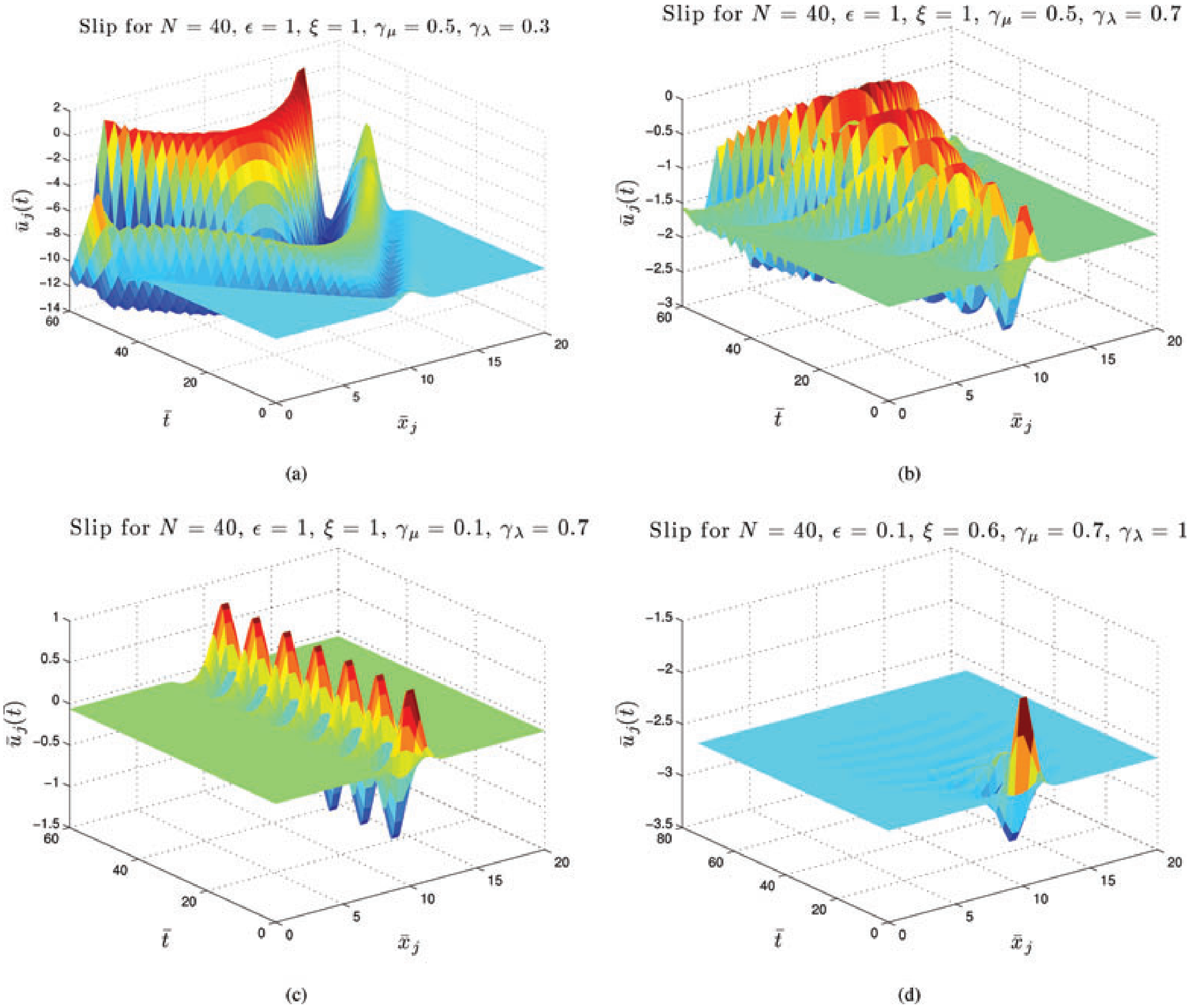

Figure 12. These four plots show the slip of a chain of 40 blocks with different parameter combinations. (a) The initial pulse split into two localized pulses that travel quickly through the medium and interact with the boundary, suggesting solitonic behaviour. (b) The initial slip pulse travels throughout the medium but the propagation is more similar to a crack, where the perturbation spreads throughout the medium until the whole chain is slipping. In (a) and (b) only the values of γ_μ^2/ξ and γ_λ^2 are varied, suggesting that the travelling pulse solutions are dependent (at least) on these parameters. (c) For a different set of parameter values, the slip remains localized in space and the amplitude maintains its height. (d) The slip remains localized but the amplitude dies out. In this case the initial slip perturbation decays over time, suggesting that under these parameter values, the friction law alone can be a mechanism to halt rupture propagation.

behaviour emerges. Initial data is assigned to both of our systems in the form of a perturbation from equilibrium given by a smooth Gaussian pulse, zero initial velocity and free boundary conditions as given in Sections 2.3 and 3.3. This initial, localized pulse is again intended to represent localized departure from equilibrium and it tends to remain localized under certain parameter values, suggesting the presence of solitonic or breather solutions. We are interested in determining the parameter(s) on which this behaviour depends.

In the next section, we find that solitary and localized behaviour seems to be dependent on the ratio between the values of the parameters defined by γ_λ^2 and γ_μ^2/ξ, indicating that the emergence of these types of solutions may be directly affected by the parameters λ and μ, (the spring constant connecting each block to the driver plate, and the spring constant between blocks in the original, discrete formulation). This coincides with the findings of Español (1994) who found the localization dependent on the speed of sound $l^2 = \frac{\mu}{\lambda}$. In the case of the localized (breather) solutions, in some parameter regimes the amplitude of this localized pulse decays over time, as viewed in Figs 12(d) and 13(d).

Fig. 12 shows four different numerical solutions to the ODEs (8) where a chain of 40 blocks is considered. In Fig. 12(a), we see that for this set of parameter values, the initial Gaussian pulse splits into two solitary waves that travel through the medium and interact with the boundary. In Fig. 12(b) however, the initial pulse does not propagate like a localized pulse, but more like a crack, where the initial perturbation spreads throughout the medium until the entire chain is slipping. Thus not all parameter combinations yield localized or solitary wave like solutions. Figs 12(c) and (d) show solutions where the slip does not propagate throughout the medium, but remains localized or quasi-localized in the centre of space, suggesting the presence of breather solutions. In these cases the slip either dies out (as in Fig. 12d), or maintains its amplitude and 'breathes' (seen in Fig. 12c).

We are interested if solitary or localized solutions occur for the PDE in eq. (12) under similar conditions to the ODEs (8), or if the

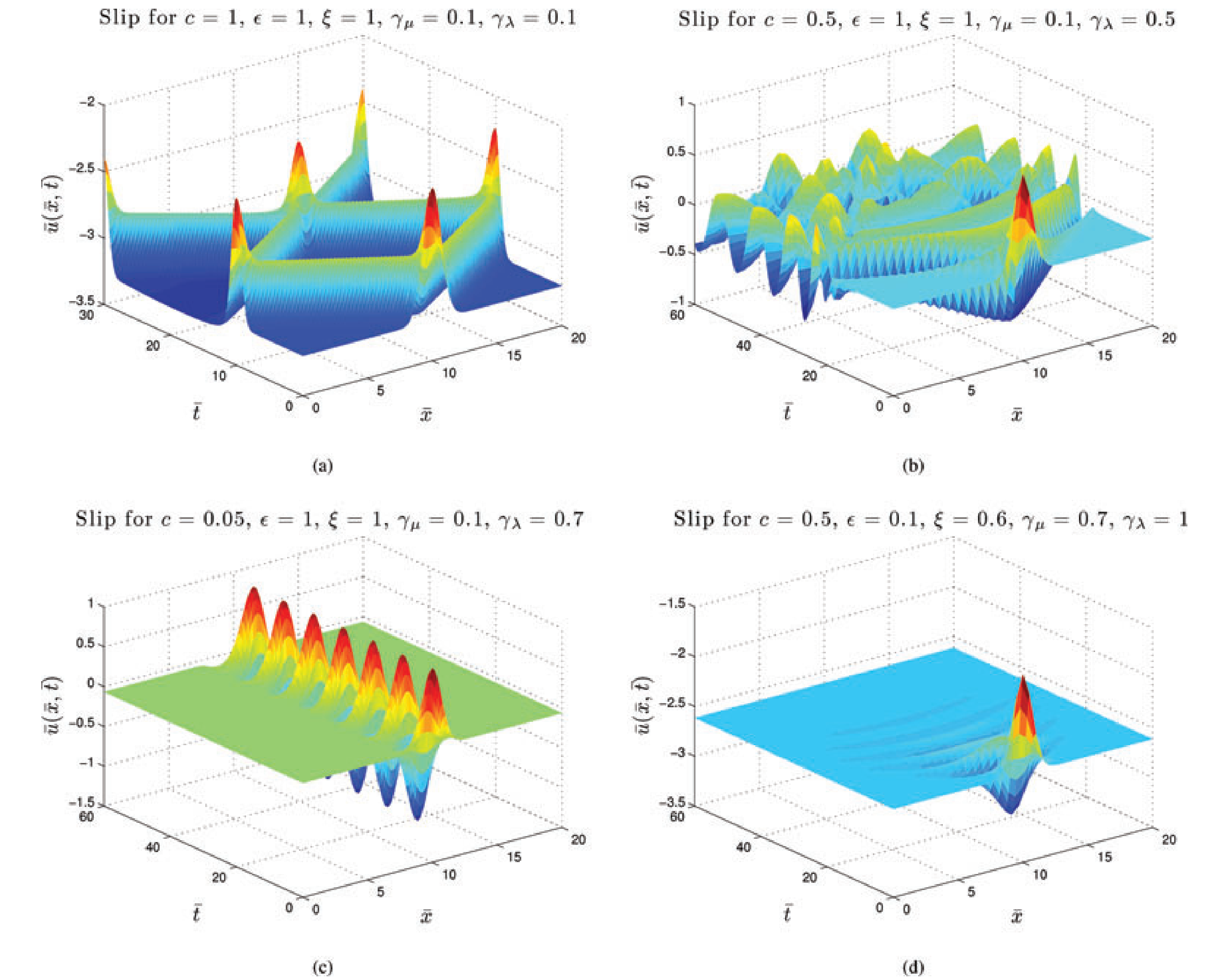

Figure 13. These four plots are the solutions to the PDE in eq. (12) corresponding to the parameter values used in the previous plot for the ODEs (a) the PDE is initialized by a centred Gaussian pulse that splits into two waves that travel quickly throughout the medium and interact with the boundary. (b) The initial slip pulse travels throughout the medium but the pulse does not remain localized. (c) For a different set of parameter values, the slip remains localized in space and the amplitude maintains its height. (d) The slip remains localized but the amplitude dies out. In this case the initial slip perturbation decays over time, suggesting that under these parameter values, the friction law alone can be a mechanism to halt rupture propagation.

qualitative behaviour changes in the continuum case. Fig. 13 shows solutions to the PDE with the same parameter values and one can see, when comparing these plots to those in Fig. 12, that for these sets of parameter values the dynamics are fairly similar, although we cannot compare them absolutely as the PDE is determined by the additional parameter c.

To investigate the behaviour when two of these solitary waves meet, we take a solution that resembles a soliton and initialize it with two smooth Gaussian pulses, with different amplitudes. Fig. 14 shows the profiles at different times for the interaction of these two pulses. We observe that each initial pulse splits into two waves that propagate through the medium, maintaining the same shape even after the interaction, suggesting solitonic behaviour.

We can study this localized behaviour in the non-linear regime by fixing the wave speed c at a constant value, and observing the behaviour of the solution when varying the driving term γ_λ^2, that is, the term corresponding to the pull of the driver plate (and the parameter responsible for loading energy into the system) and the damping term γ_μ^2/ξ, the parameter controlling the amount of friction acting on the system. With these parameters in mind, we can control the behaviour of the system by means of a single perturbation parameter,

$$\zeta = \frac{\text{drive}}{\text{damping}} = \frac{\gamma_\lambda^2}{\gamma_\mu^2/\xi} = \frac{\gamma_\lambda^2 \xi}{\gamma_\mu^2},$$

the ratio of the drive to the damping.

We are interested in determining the role that ζ plays in the emergence of these travelling waves or localized solutions. Fig. 15 shows results from the solutions to the PDE in eq. (12) in a parameter-varying study. Since increasing the control parameter ζ is analogous to keeping all parameters fixed except for γ_λ^2 or γ_μ^2/ξ, these figures demonstrate the effect that the control parameter has on the system. Fig. 15 shows a set of nine plots of solutions to the PDE when the control parameter $\zeta = \gamma_\lambda^2/({\gamma_\mu}^2/\xi)$ is increased (from left to right, or from bottom to top). One can observe that the plots

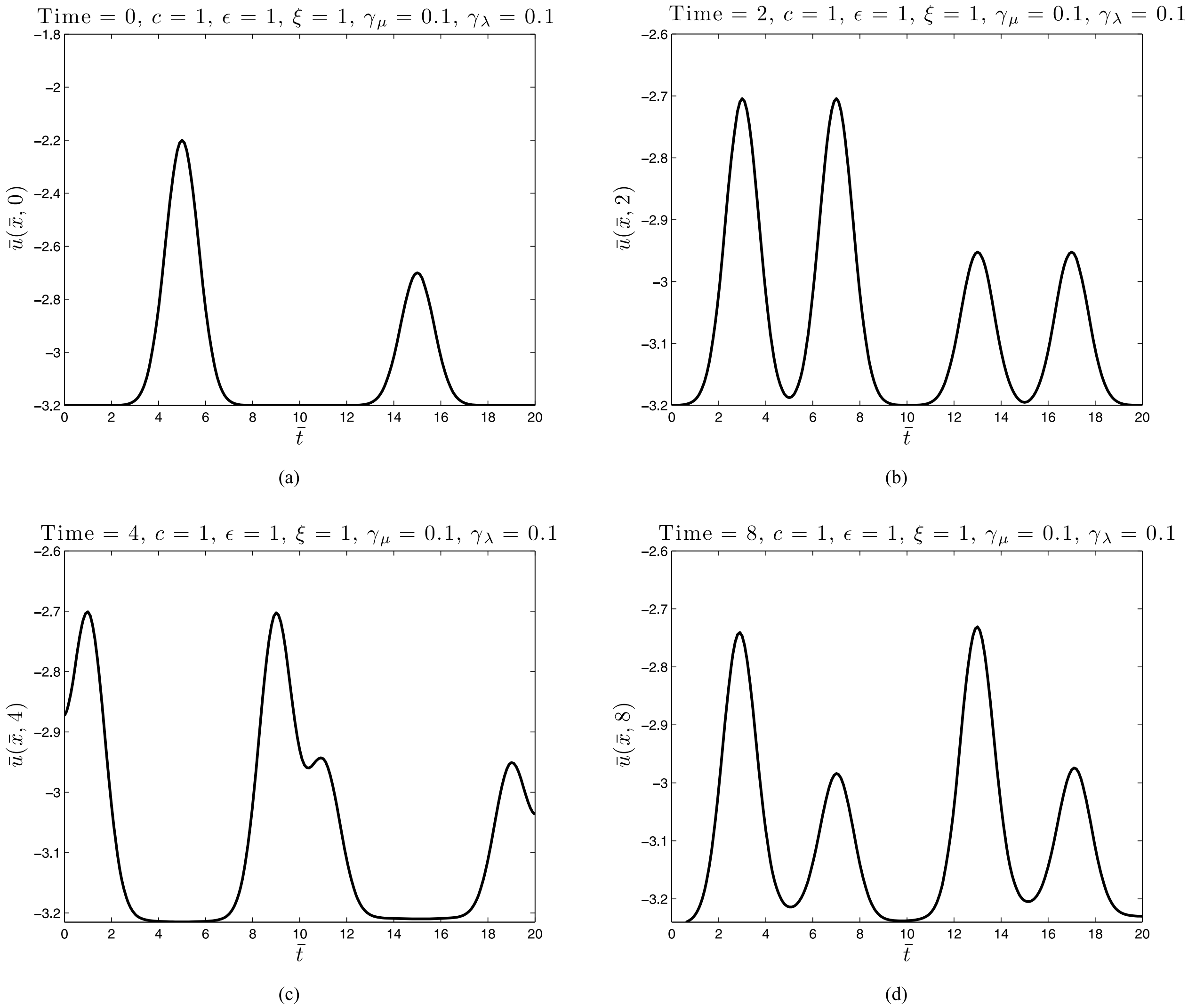

Figure 14. Four plots showing the slip profile at different times, resembling the qualitative behaviour of a soliton. (a) Initialized with two smooth Gaussian pulses. (b) Each wave splits into two waves that maintain the same shape after they pass through each other, seen in (c) and (d), suggesting solitonic behaviour.

in the left column illustrate how the initial Gaussian pulse splits into two waves that travel outwards through the boundary. But in moving from left to right (or from bottom to top), the slip pulse is squeezed together so that it takes longer to interact with the boundary. This is evidence that an increase in the control parameter will cause the slip to localize, and if ζ is further increased, the pulse will be damped out (as seen in the column on the right of Fig. 15). This makes sense as one can consider increasing ζ as analogous to increasing γ_μ (effectively increasing the pull of the driver plate so that it forces the chain of blocks to slide at steady state). Thus the localized solutions seem to be dependent on a balance between the drive and damping parameters. One can further view this effect as analogous to crossing under the Hopf bifurcation plane seen in Fig. 16, where parameter combinations yield stationary solutions.

4.4 Analytical investigation of soliton solutions

In this section, we investigate whether we can analytically determine the parameter spaces for which these solitary wave solutions occur.

The original PDE (written with wave speed c) is

$$\left.\begin{aligned}\frac{\partial^2\bar{u}}{\partial\bar{t}^2} &= c^2\frac{\partial^2\bar{u}}{\partial\bar{x}^2} - \gamma_\lambda^2\bar{u} - \left(\gamma_\mu^2/\xi\right)\left(\bar{f} + \bar{\Theta} + \ln\left(\frac{\partial\bar{u}}{\partial\bar{t}} + 1\right)\right)\\ \frac{\partial\bar{\Theta}}{\partial\bar{t}} &= -\left(\frac{\partial\bar{u}}{\partial\bar{t}} + 1\right)\left(\bar{\Theta} + (1+\epsilon)\ln\left(\frac{\partial\bar{u}}{\partial\bar{t}} + 1\right)\right)\end{aligned}\right\}. \tag{13}$$

We now consider a solution to (13) of the form $h(\bar{x} + c_o\bar{t})$, that is, a soliton travelling solution with wave speed c_o. Letting $\psi = \bar{x} + c_o\bar{t}$, and plugging h into the PDE yields the following ODE

$$\left.\begin{aligned}\left(c_o^2 - c^2\right)\frac{d^2h}{d\psi^2} &= -\gamma_\lambda^2 h - \left(\gamma_\mu^2/\xi\right)\left(\bar{f} + \bar{\Theta} + \ln\left(c_o\frac{dh}{d\psi} + 1\right)\right)\\ c_o\frac{d\bar{\Theta}}{d\psi} &= -\left(c_o\frac{dh}{d\psi} + 1\right)\left(\bar{\Theta} + (1+\epsilon)\ln\left(c_o\frac{dh}{d\psi} + 1\right)\right)\end{aligned}\right\}. \tag{14}$$

This second-order ODE can be rewritten as a system of first-order ODEs by letting $v = \frac{dh}{d\psi}$.

$$\left.\begin{aligned}\frac{dh}{d\psi} &= v\\ \left(c_o^2 - c^2\right)\frac{dv}{d\psi} &= -\gamma_\lambda^2 h - \left(\gamma_\mu^2/\xi\right)\left(\bar{f} + \bar{\Theta} + \ln(c_o v + 1)\right)\\ \frac{d\bar{\Theta}}{d\psi} &= -\frac{1}{c_o}(c_o v + 1)(\bar{\Theta} + (1+\epsilon)\ln(c_o v + 1))\end{aligned}\right\}. \tag{15}$$

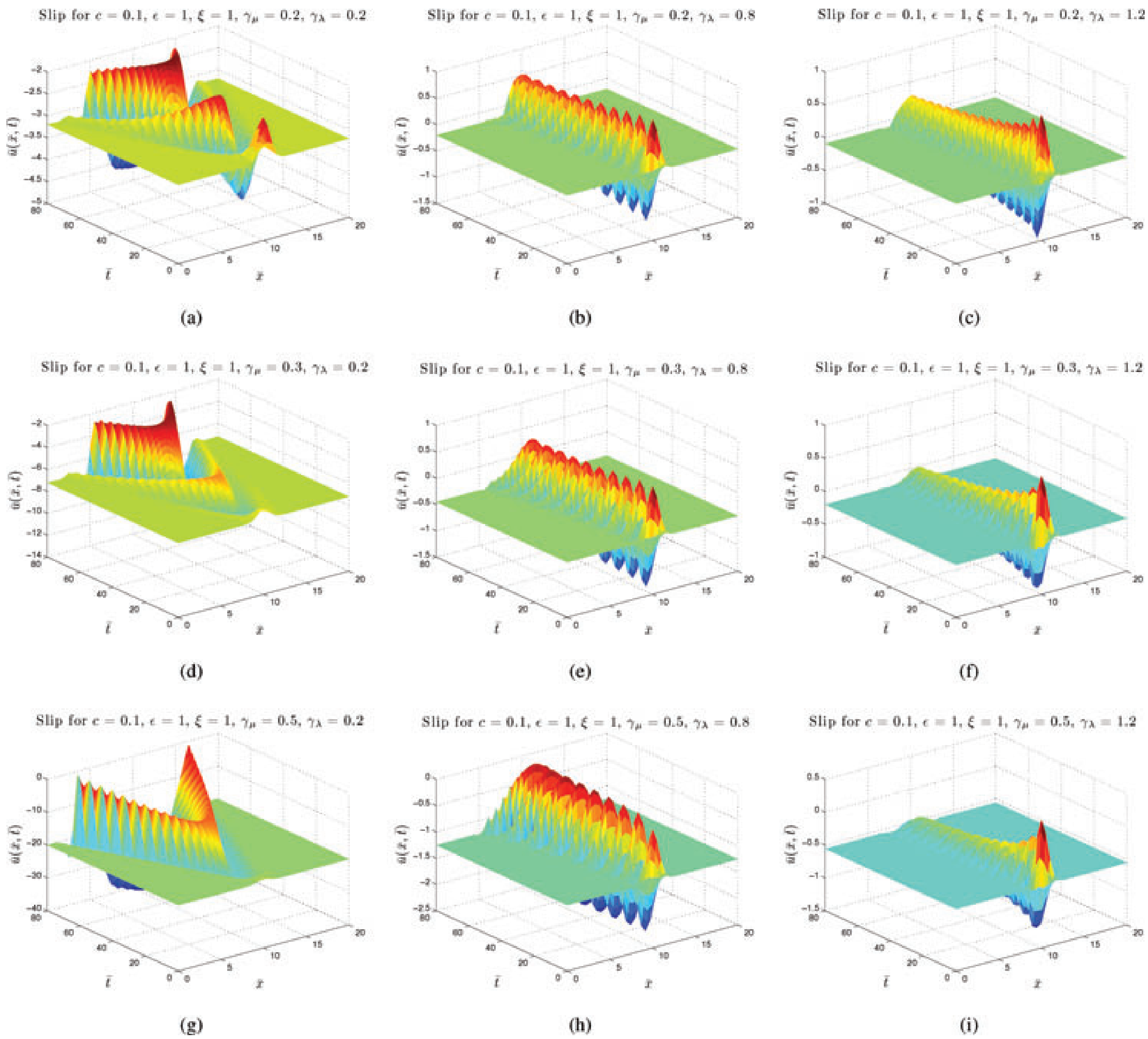

Figure 15. For the continuum model, these nine plots show the localization of slip as a function of the control parameter ζ (the ratio of drive to damping parameters). Moving from left to right (or bottom to top) corresponds to increasing the value of $\zeta = \gamma_\lambda^2/(\gamma_\mu{}^2/\xi)$. Moving from left to right we see that increasing the drive tends to squeeze the pulse together, and also decay the pulse's amplitude. Moving from top to bottom however shows that increasing the damping term causes the pulse to delocalize much faster, and (at least in the case of the far left column) causes the pulse to split into two waves that travel like a soliton.

To do stability analysis of the ODE (15), we look at the Jacobian matrix of eq. (15)

$$Df = \begin{bmatrix} 0 & 1 & 0 \\ \frac{-\gamma_\lambda^2}{c_o^2 - c^2} & \frac{-\gamma_\mu^2 c_o}{\xi(c_o^2 - c^2)(c_o v + 1)} & \frac{-\gamma_\mu^2}{\xi(c_o^2 - c^2)} \\ 0 & -(\bar{\Theta} + (1+\epsilon)(1 + \ln(c_o v + 1))) & -\frac{c_o v + 1}{c_o} \end{bmatrix}$$

and Df evaluated at the stationary solution $(h, v, \Theta) = \left(-\frac{\gamma_\mu^2 \bar{f}}{\xi \gamma_\lambda^2}, 0, 0\right)$ yields

$$J = \begin{bmatrix} 0 & 1 & 0 \\ \frac{-\gamma_\lambda^2}{c_o^2 - c^2} & \frac{-\gamma_\mu^2 c_o}{\xi(c_o^2 - c^2)} & \frac{-\gamma_\mu^2}{\xi(c_o^2 - c^2)} \\ 0 & -(1+\epsilon) & -\frac{1}{c_o} \end{bmatrix}.$$

It is important to note that with a few assumptions made for the values of the parameters c and c_0, matrix J is analogous to matrix A obtained in Erickson *et al.* (2008), for the equations governing a single block and a similar bifurcation analysis can be done (see Erickson *et al.* 2008, for more details): matrix J has three distinct eigenvalues: one real eigenvalue and two complex conjugates. When the real part of the complex conjugates crosses the imaginary axis, the system in eq. (15) undergoes a Hopf bifurcation from a stationary solution into a periodic orbit [see (Guckenheimer & Holmes 1983; Perko 2001)], as occurred in the single-block case in Erickson *et al.* (2008).

Fig. 16 shows the parameter combinations that will yield bifurcations of the stationary state. Not surprisingly, it appears similar to the surface computed in Erickson *et al.* (2008) for the single block case, thus a similar analysis of the bifurcation plane can be made. Parameter combinations that lie below this plane will generate stationary solutions to eq. (15), but once the parameter values have crossed this Hopf bifurcation plane, we see either solitary wave type solutions or localized solutions like those in the Figs 12(a)–(c) and 13(a)–(c). We can use the information obtained from the study of the single block [see Erickson *et al.* (2008)] to predict that a similar route to chaos exists for the ODE (15) derived from considering soliton solutions to the PDE (11). In this case, increasing the value of the parameter ϵ will correspond to a period doubling cascade into chaos, resulting in solitary wave solutions that are

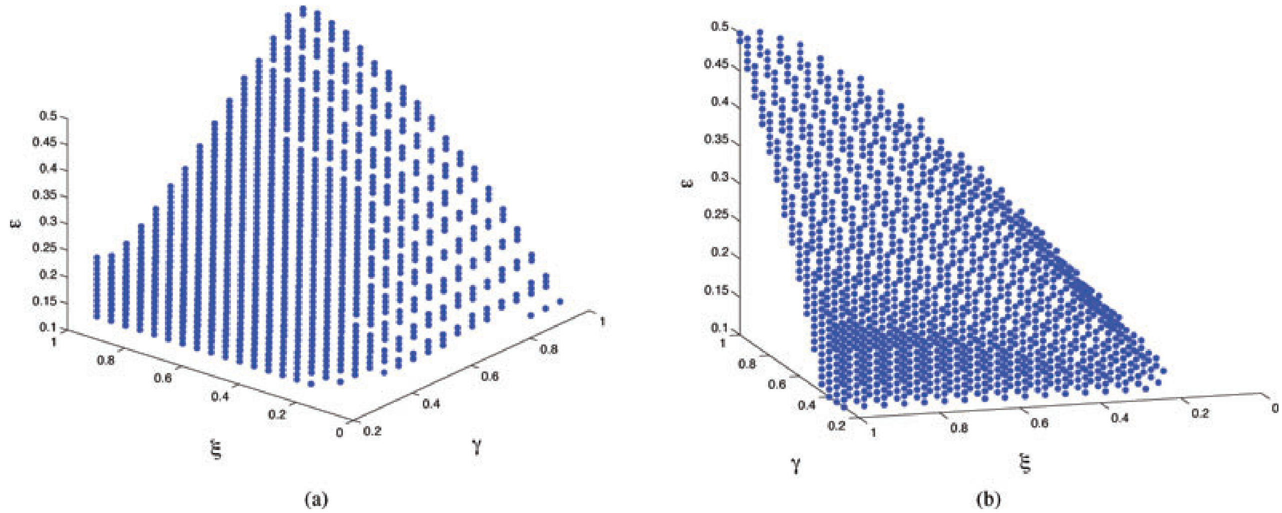

Figure 16. (a) and (b) show two different views of the bifurcation surface associated with eq. (15), where $\gamma := \gamma_\mu = \gamma_\lambda$. Parameter combinations that lie below the surface will generate stationary solutions, while a combination above the surface will correspond to a Hopf bifurcation, and yield a periodic orbit. That it is a skewed surface for the parameter space we consider implies that the Hopf bifurcation is dependent on all three parameters ϵ, ξ and γ.

aperiodic in time, although ϵ will need to be on the order of ≈ 11, as before. The assertion of this result would suggest that solitary wave-type solutions in the continuum formulation undergo behavioural changes on the same order of parameter values as in the single block case.

5 DISCUSSION: IMPLICATIONS ON THE SCALING OF THE FRICTION LAW

It has been widely recognized that our understanding of the physical mechanisms controlling earthquake rupture depends significantly on understanding the role of friction (see Brace & Byerlee 1966; Scholz 1998, among others). We believe that earthquakes and the resulting ground motions are affected by at least four factors, including initial stress, fault geometry, fault frictional behaviour and wave-propagation path effects. Of these, geometry and wave-propagation are somewhat possible to predetermine, the spatial distribution of the initial stress can be modelled according to the stochastic model discussed in Lavallée *et al.* (2006) (for applications see Schmedes *et al.* 2010a,b), but fault friction is still a major unknown. This makes the knowledge of fault friction a cornerstone of understanding earthquake behaviour. As highlighted in Harris (2004), earthquakes are the result of processes in the earth's crust that have evolved over multiple scales in both time and space. Understanding the physics of earthquakes requires the study of these processes at all scales from both an observational and a dynamic modelling perspective.

That the transition to chaos for the discrete and continuum model with the slip law formulation of rate-and-state friction ensues for a smaller parameter value than in the case of a single block may be an indication that a careful rescaling of the friction law is necessary, prior to attaching the friction law to full scale models. A similar conclusion was made by Schmittbuhl *et al.* (1996) who studied a 'hierarchical array of blocks' and found that velocity weakening friction was scale dependent. These authors studied the bulk response of a 2-D elastic body sheared over a rough surface defined by a the velocity weakening friction law. They found that this friction law can produce Coulomb-like behaviour at the system scale. More specifically, the velocity dependence of the body at the interface is lost or blurred when moving to larger scales. They conclude by emphasizing the need to study scale dependent effects of friction laws with an intrinsic length scale. Our results suggest that when implementing rate-and-state friction in dynamic rupture models, it is possible that qualitative behaviour can be lost or altered when considering full-scale models. However it is possible to investigate the evolution of the scaling properties of numerical solutions to equations involving the friction law. Unfortunately, the presence of non-linear terms in the mathematical formulation of friction laws like the one considered here makes it very difficult to define a transformation from laboratory scales to full scale models of the earth's faults. Another hypothesis will consist of formulating an 'effective friction law' for length scales on the order of 100 m, much like the pioneering work of Campillo *et al.* (2001) who explored how small-scale variability in the parameters of the friction law can be renormalized to larger length scales.

6 CONCLUSIONS

We have derived the equations for both the discrete and the continuous formulations of a 1-D Burridge & Knopoff (1967) spring-block model subject to the slip law version of the rate-and-state friction law. In the discrete case we observe a transition to chaos when varying the system size, that is, the number of blocks N. For $N < 20$ blocks, periodic behaviour emerges. When N is increased to 20 however, this periodic behaviour is lost and chaos ensues, as further asserted by the broad-band noise in the power spectrum (see Fig. 6) and the presence on a positive maximal Lyapunov exponent (see Fig. 7). This transition occurs for a fixed set of parameter values and we see that the small value of $\epsilon = 0.5$ will generate chaotic motion, as long as the system size N is sufficiently large. This value is much smaller than that required for chaotic motion that we found in the single block case (Erickson *et al.* 2008), where $\epsilon \approx 11$. This suggests that, in contrast to the conclusions made by Lapusta & Rice (2003) who found only periodic behaviour emerging from rate-and-state friction, dynamic rupture modelling with this friction law can produce chaotic dynamics when considering a wide range of parameter values with an increase in system size.

Also, these results suggest that chaotic regimes in the BK model under the slip law version of rate-and-state friction is a function of the number of blocks considered, similar to the conclusions of

Schmittbuhl *et al.* (1993) who studied a similar block-spring model subject to a velocity weakening friction law and found that chaos was also dependent on the system size. It should be emphasized that this information reveals that this friction law may very well be scale-dependent, as we have seen different dynamics emerge in systems with different numbers of blocks. That the transition to chaos appears highly sensitive to the number of blocks N as well as the value of the parameter ϵ suggests that one should take into consideration their system size when choosing the parameters for a dynamic rupture model, or find another means of scaling the friction law appropriately. Because chaotic solutions appear for smaller values of this specific parameter than in the case for a single block, it is probable that chaotic dynamics emerge for a broader range of parameter values for systems of larger size.

For the continuum model derived from this spring-block model subject to the slip law version of rate-and-state friction, a bifurcation from a stationary state (steady sliding), to periodic, to chaotic behaviour can be observed when the parameter ϵ is increased, as further asserted in the power spectrum (see Fig. 11). Recall that ϵ is the ratio of the stress parameters $(B - A)$ and A in the rate-and-state friction law. Our results in this section show that $\epsilon = 0.4$ is sufficient for chaos in the PDE, a much smaller value than that required for chaotic motion in the single block system in Erickson *et al.* (2008), where $\epsilon \approx 11$. Although it is difficult to compare absolutely the discrete and the continuum model due to the second model's additional parameter c, in either case the critical value for ϵ is much smaller than in the case of a single block, where $\epsilon \approx 11$. Our numerical solutions so far suggest that the critical value of the parameter ϵ necessary to induce chaos decreases as a function of N, the numbers of blocks considered. In the future it will be interesting to find the relationship between N and the critical value for ϵ, while keeping the other parameters fixed [for a hypothetical curve, see fig. 25 in Erickson (2010)]. In particular, it will be important to establish if this relationship depends on the values taken by the other parameters. Given the scale size of the model, the corresponding value taken by ϵ could be a useful method for controlling the observation of periodic or chaotic earthquake ruptures.

Furthermore, when we consider that $\epsilon = 1/S$, where S is the non-dimensional seismic ratio (Andrews 1976), smaller values of ϵ that yield chaotic dynamics correspond to a broader range of S values. We found that in the single-block case, critical values of ϵ were large, corresponding to $S \approx \frac{1}{10}$ or smaller. Although we concluded in Erickson *et al.* (2008) that earthquake ruptures generated by chaotic simulations from a single block model correspond to velocities propagating at the supershear speed (see among others, Freund 1979; Dunham 2007), for these models with more than one block chaotic regimes can be reached for a larger range of S values. In these cases, we find chaotic regimes corresponding to $S = 2$ or smaller.

In addition to these transitions from periodic to chaotic behaviour, we have also observed that both the discrete and the continuous formulation of the Burridge–Knopoff spring-block model under the slip law version of rate-and-state friction exhibit solutions where an initial, smooth Gaussian pulse can either split into two travelling waves that propagate as solitons, or remain localized in space, as breathers. In spite of having only explored a small region of the parameter space, we were able to determine which internal parameters seem to affect this behaviour. Because these solitonic or localized solutions can be understood as a proxy for the propagation of the rupture across the fault during an earthquake (Heaton 1990), this result may also suggest a possible range for parameters that could be used in future earthquake modelling. By narrowing the parameter space to values that yield localized solutions, we may have a method for assigning appropriate values to parameters that have, thus far, been difficult to determine.

Furthermore, a robust friction law is vital for dynamic rupture modelling of earthquakes, but evokes the question of whether or not small-scale laboratory derived friction laws are appropriate for full-scale modelling and modelling at high slip speeds. We have shown that finding pulse-like solutions in the continuum model reduces to studying the bifurcation analysis of a single block. Thus it is possible that using parameters relevant to the single block case under rate-and-state friction may be directly applicable to large-scale models if one is interested in generating pulse-like solutions. This knowledge could be an indirect way for validating the use of a small-scale, laboratory derived friction law in full-scale dynamic rupture models.

An additional observation we made in this study is that for certain parameter combinations, the initial slip pulse in the BK model with rate-and-state friction tends to die over time (as in the plots in the bottom right of Figs 12 and 13). Now the earthquake rupture process can be roughly divided into three parts: nucleation, propagation and arrest. But although rupture can be initiated in dynamic models of earthquakes by stress perturbations in initial conditions, an appropriate technique for terminating rupture is still unclear. Many dynamic models of earthquakes impose an artificial mechanism for stopping the rupture. The stopping criterion invoked by Ma *et al.* (2008) for example, solves for a traction value that will force the slip rate to die at the next time step during the dynamic rupture. The dying pulse in the bottom right plot of Figs 12 and 13 suggest that the friction law alone can provide a sufficient mechanism for halting the rupture process. In these cases where the slip amplitude decays, the dying pulse suggests that a localized rupture can propagate along the fault and be attenuated over a finite fault length. The plots in the bottom right of Figs 12 and 13 suggest that properly choosing parameters of the friction law will be sufficient in halting rupture propagation. Having determined the parameter responsible for causing the slip to decay naturally, this parameter can be made a function of time and/or space to have a method for dynamically terminating slip events.

Under the slip law formulation of rate-and-state friction, we may have discovered only a small subset of solutions to both the discrete and the continuous model, but there is no question that even in one spatial dimension, a rich phenomenology of dynamics exists. Furthermore, the presence of chaotic regimes and localized solutions are of great importance because they help justify the use of a relatively simple model in studies of fault friction, whereas more sophisticated dynamic models may be computationally limited.

ACKNOWLEDGMENTS

The authors would like to thank Hiroyuki Noda and the other anonymous reviewer for their thoughtful and detailed reviews of this manuscript, as well as Raúl Madariaga for his insight regarding this work. This material is based upon work supported by the National Science Foundation under Award No. 0948304 and Grant No. 0738954. This research was supported by the Southern California Earthquake Center. The research has been partially supported by SCEC Grant No. 572726 as well as UCSB matching funds for SCEC. SCEC is funded by NSF Cooperative Agreement EAR - 0529922 and USGS Cooperative Agreement 07HQAG0008. This is SCEC contribution number 1492. This is ERI contribution No. 1012.

REFERENCES

Ampuero, J.-P. & Rubin, A.M., 2007. Earthquake nucleation on rate and state faults - aging and slip laws, *J. geophys. Res.,* **113,** 1–21.

Andrews, D.J., 1976. Rupture velocity of plane strain shear cracks, *J. geophys. Res.,* **81,** 5679–5687.

Ascher, U.M. & Petzold, L.R., 1998. *Computer Methods for Ordinary Differential Equations and Differential- Algebraic Equations,* 1st edn, SIAM.

Birnir, B., 1994. Qualitative analysis of radiating breathers, *Comm. Pure appl. Math.,* **47,** 103–119.

Birnir, B., McKean, H. & Weinstein, A., 1994. The rigidity of sine-Gordon breathers, *Comm. Pure appl. Math.,* **47,** 1043–1051.

Brace, W.F. & Byerlee, J.D., 1966. Stick-slip as a mechanism for earthquakes, *Science,* **153,** 990–992.

Burridge, R. & Knopoff, L., 1967. Model and theoretical seismicity, *Bull. seism. Soc. Am.,* **57,** 341–371.

Campillo, M., Favreau, P., Ionescu, I.R. & Voisin., C., 2001. On the effective friction law of a heterogeneous fault, *J. geophys. Res.,* **106,** 16 307–16 322.

Carlson, J.M. & Langer, J., 1989. Mechanical model of an earthquake fault, *Phys. Rev. A,* **40,** 6470–6484.

Carlson, J.M., Langer, J.S., Shaw, B.E. & Tang, C., 1991. Intrinsic properties of a burridge-knopoff model of an earthquake fault, *Phys. Rev. A,* **44**(2), 884–897.

Corish, S.M., Bradley, C.R. & Olsen, K.B., 2007. Assessment of a nonlinear dynamic rupture inversion technique applied to a synthetic earthquake, *Bull. seism. Soc. Am.,* **97,** 901–914.

Daub, E.G. & Carlson, J.M., 2008. A constitutive model for fault gouge deformation in dynamic rupture simulations, *J. geophys. Res.,* **113,** B12309, doi:10.1029/2007JB005377.

Dieterich, J., 1978. Time-dependent friction and the mechanics of stick-slip, *Pure appl. Geophys.,* **116,** 790–806.

Dieterich, J.H., 1979. Modeling of rock friction, 1, experimental results and constitutive equations, *J. geophys. Res.,* **84,** 2161–2168.

Dieterich, J.H. & Kilgore, B.D., 1994. Direct observation of frictional contacts: new insights for state dependent properties, *Pure appl. Geophys.,* **143,** 283–302.

Dunham, E.M., 2007. Conditions governing the occurrence of supershear rupture under slip weakening friction, *J. geophys. Res.,* **112,** B07302, doi:10.1029/2006JB004717.

Elbanna, A.E. & Heaton, T., 2009. Statistics of a dynamical system failing at multiple length scales and its implications on material strength, Poster presented at the Southern California Earthquake Center (SCEC) annual meeting, Palm Springs, California 2009 September 12–16, abstract published in Proceedings and Abstracts, Volume XIX.

Erickson, B., 2010. Complexity in the nonlinear Dieterich-Ruina friction law, *PhD thesis*, University of California, Santa Barbara.

Erickson, B., Birnir, B. & Lavallée, D., 2008. A model for aperiodicity in earthquakes, *Nonlin. Processes Geophys.,* **15,** 1–12.

Erickson, B., 2010. Complexity in the nonlinear Dieterich-Ruina friction law, *PhD thesis*, University of California, Santa Barbara.

Erickson, B., Birnir, B. & Lavallée, D., 2008. A model for aperiodicity in earthquakes, *Nonlin. Processes Geophys.,* **15,** 1–12.

Español, P., 1994. Propagative slipping modes in a spring-block model, *Phys. Rev. E,* **50,** 227–235.

Freund, L.B., 1979. The mechanics of dynamic shear crack propagation, *J. geophys. Res.,* **84**(B5), 2199–2209.

Frisch, U., 1995. *Turbulence: The Legacy of A.N. Kolmogorov,* 1st edn, Cambridge University Press, Cambridge.

Guckenheimer, J. & Holmes, P., 1983. *Nonlinear Oscillations, Dynamical Systems, and Bifurcations of Vector Fields,* 1st edn, Springer-Verlag, New York, NY.

Gustafsson, B., 2008. *High Order Difference Methods for Time Dependent PDE,* Springer Series in Computational Mathematics, 1st edn, Springer, New York, NY.

Harris, R., 2004. Numerical simulations of large earthquakes: dynamic rupture propagation on heterogeneous faults, *Pure appl. geophys.,* **161,** 2171–2181.

Heaton, T.H., 1990. Evidence for and implications of self-healing pulses of slip in earthquake rupture, *Phys. Earth. planet. Inter.,* **64,** 1–20.

Kichenassamy, S., 1991. Breathers and the sine-Gordon equation, *Am. Math. Soc.,* **122,** 73–76.

Lapusta, L. & Rice, J., 2003. Nucleation and early seismic propagation for small and large events in a crustal earthquake model, *J. geophys. Res.,* **108,** 1–18.

Lavallée, D., Liu, P. & Archuleta, R.J., 2006. Stochastic model of heterogeneity in earthquake slip spatial distributions, *Geophys. J. Int.,* **165,** 622–640.

Ma, S., Custódio, S., Archuleta, R.J. & Liu, P., 2008. Dynamic modeling of the 2004 Mw 6.0 Parkfield, California, earthquake, *J. geophys. Res.,* **113,** 1–16.

Madariaga, R., 1998. Study of an oscillator of single degree of freedom with Dieterich-Ruina rate and state friction, *Unpublished Notes* (Preprint).

Madariaga, R. & Olsen, K.B., 2002. Earthquake dynamics, in *International Handbook of Earthquake and Engineering Seismology,* Vol. 81A, pp. 175–194, eds Lee, W.H.K., Kanamori, H., Jennings, P.C. & Kisslinger, C., Academic Press, London.

Marone, C., 1998. Laboratory-derived friction laws and their application to seismic faulting, *Annu. Rev. Earth Planet. Sci.,* **26,** 643–696.

Mickens, R.E., 2004. *Mathematical Methods for Natural and Engineering Sciences,* 1st edn, World Scientific, Singapore.

Nakatini, M., 2001. Conceptual and physical clarification of rate and state friction: frictional sliding as a thermally activated rheology, *J. geophys. Res.,* **106**(B7), 13 347–13 380.

Noda, H., Dunham, E.M. & Rice, J.R., 2009. Earthquake ruptures with thermal weakening and the operations of major faults at low overall stress levels, *J. geophys. Res.,* **114,** B07302, doi:10.1029/2008JB006143.

Ohnaka, M. & Shen, L.-F., 1999. Scaling of the shear rupture process from nucleation to dynamic propogation: implications of geometric irregularity of the rupturing surfaces, *J. geophys. Res.,* **104,** 817–844.

Oseledec, V., 1968. A multiplicative ergodic theorem: Lyapunov characteristic numbers for dynamical systems, *Trans. Moscow Math. Soc.,* **19,** 197–231.

Pain, H.J., 1968. *The Physics of Vibrations and Waves,* 2nd edn, John Wiley & Sons, Ltd., Chichester.

Perko, L., 2001. *Differential Equations and Dynamical Systems,* 3rd edn, Springer-Verlag, New York, NY.

Peyrat, S., Olsen, K. & Madariaga, R., 2004. Which dynamic rupture parameters can be estimated from strong ground motion and geodetic data?, *Pure appl. geophys.,* **161,** 2155–2169.

Putelat, T., Willis, J.R. & Dawes, J.H.P., 2008. On the seismic cycle seen as a relaxation oscillation, *Phil. Mag.,* **88**(28–29), 3219–3243.

Rabinowicz, E., 1951. The nature of the static and kinetic coefficients of friction, *J. Appl. Phys.,* **22,** 1373–1379.

Rice, J.R., 1983. Constitutive relations for fault slip and earthquake instabilities, *Pure appl. Geophys.,* **121,** 443–475.

Rice, J.R., 1993. Spatio-temporal complexity of slip on a fault, *J. geophys. Res.,* **98,** 9985–9907.

Rice, J.R., 2006. Heating and weakening of faults during earthquake slip, *J. geophys. Res.,* **111,** B05311, doi:10.1029/2005JB004006.

Rice, J.R. & Ruina, A.L., 1983. Stability of steady-frictional slipping, *J. Appl. Mech.,* **50,** 343–349.

Rice, J.R., Lapusta, N. & Ranjith, K., 2001. Rate and state dependent friction and the stability of sliding between elastically deformable solids, *J. Mech. Phys. Solids,* **49,** 1865–1898.

Rojas, O., Dunham, E.M., Day, S.M., Dalguer, L. & Castillo, J.E., 2009. Finite difference modeling of rupture propagation with strong velocity-weakening friction, *Geophys. J. Int.,* **179,** 1831–1858.

Ruina, A., 1983. Slip instability and state variable friction laws, *J. geophys. Res.,* **88,** 10359–10370.

Sandri, M., 1996. Numerical calculation of Lyapunov exponents, *Math. J.,* **6,** 78–84.

Schmedes, J., Archuleta, R.J. & Lavalleé, D., 2010a. Correlation of earthquake source parameters inferred from dynamic rupture simulations, *J. geophys. Res.,* **115,** doi:10.1029/2009JB006689.

Schmedes, J., Archuleta, R.J. & Lavalleé, D., 2010b. Dependency of supershear transition and ground motion on the autocorrelation of initial stress, *Tectonophysics,* **493,** 222–235, doi:10.1016/j.tecto.2010.05.013.

Schmittbuhl, J., J.-P., V. & Roux, S., 1993. Propagative macrodislocation modes in an earthquake fault model, *Europhys. Lett.,* **21**(3), 375–380.

Schmittbuhl, J., Vilotte, J.-P. & Roux, S., 1996. Velocity weakening friction: a renormalization approach, *J. geophys. Res.,* **101,** 13 911–13 917.

Scholz, C.H., 1998. Earthquakes and friction laws, *Nature,* **391,** 37–42.

Scholz, C.H., 2002. *The Mechanics of Earthquakes and Faulting,* 2nd edn, Cambridge University Press, Cambridge.

Sigeti, D.E., 1995. Exponential decay of power spectra at high frequency and positive Lyapunov exponents, *Physica D,* **82,** 136–153.

Turcotte, D., 1997. *Chaos and Fractals in Geology and Geophysics,* 2nd edn, Cambridge University Press, Cambridge.

Valsakumar, M.C., Satyanarayana, S.V.M. & Sridhar, V., 1997. Signature of chaos in power spectrum, *Pramana J. Phys.,* **48**(1), 69–85.

Verhulst, F., 2000. *Nonlinear Differential Equations and Dynamical Systems,* 2nd edn, Springer-Verlag, Berlin.

Zhang, W., Iwata, T., Irikura, K., Sekiguchi, H. & Bouchon, M., 2003. Heterogeneous distribution of the dynamic source parameters of the 1999 Chi-Chi, Taiwan, earthquake, *J. geophys. Res.,* **108,** 1–14.